Thermosensitive Hybrid Elastin-like Polypeptide-Based ABC Triblock Hydrogel

Michèle Dai, Guillaume Goudounet, Hang Zhao, Bertrand Garbay, Elisabeth Garanger, Gilles Pecastaings, Xavier Schultze, Sébastien Lecommandoux

Thermosensitive hybrid elastin-like polypeptide-based ABC triblock hydrogel

Michèle Dai[1,2] Guillaume Goudounet,[1] Hang Zhao,[1] Bertrand Garbay,[1] Elisabeth Garanger[1] Gilles Pecastaings,[1] Xavier Schultze[2] and Sébastien Lecommandoux*[,1]

[1] Univ. Bordeaux, CNRS, Bordeaux INP, LCPO, UMR 5629, F-33600, Pessac, France

[2] L'Oréal Recherche Avancée, 1 avenue Eugène Schueller, 93600, Aulnay-sous-Bois, France
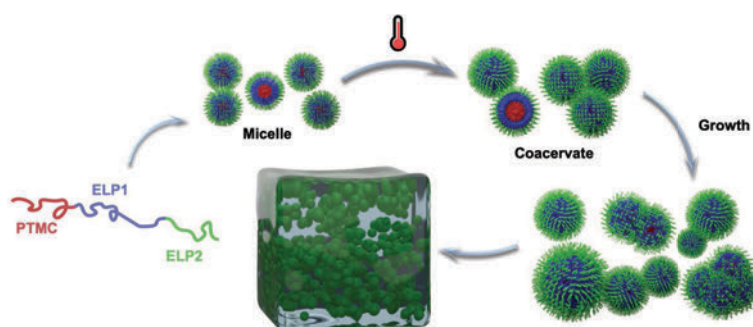
ABSTRACT

We report the synthesis of a well-defined hybrid ABC triblock terpolymer containing a synthetic poly(trimethylene carbonate) (PTMC) block A and a thermosensitive BC diblock of recombinant elastin-like polypeptides (ELPs). The triblock in diluted solution (0.1-0.3 %w/v), at low temperature in ultrapure water, forms micellar structures of 10 to 60 nm sizes in diameter as characterized by dynamic light scattering (DLS) and liquid atomic force microscopy (AFM). While heated above its transition temperature (Tt), larger particles of 200-300 nm sizes are

obtained, consistent with the formation of coacervates. When concentrated, the viscosity of the triblock copolymer solution progressively increases, giving a free-standing gel at 4 %w/v formed by a network of micron-sized particles. The formed hydrogels are thermally reversible, and their sol-gel transitions are fast and sharp. The gel formation mechanism appears to interestingly biomimic tropoelastin, the native monomeric form of natural elastin, as demonstrated by optical and cryogenic-scanning electron microscopy (cryo-SEM) imaging.

INTRODUCTION

Hydrogels result from the formation of a three-dimensional (3D) network of hydrophilic polymer chains that can swell in aqueous solution without dissolution, with broadly tunable characteristics. They are commonly classified in two main categories: "chemical" and "physical" hydrogels. Chemical hydrogels are formed by interconnected chains with permanent covalent bonds, whereas physical hydrogels are obtained by reversible non-covalent interactions such as hydrophobic, ionic or hydrogen bonds.[1–3] Reversible physical hydrogels are particularly appealing as they can exhibit sol-gel transitions in response to external *stimuli*. A wide variety of *stimuli* have been considered, but temperature is one of the most common and easy to process parameter, for biomaterials design.[4,5] In such system, a critical temperature corresponding to a phase transition, associated to a change in solvent affinity for the polymer chains, is observed. If this phase separation occurs above the critical temperature, the polymer exhibits a lower critical solution temperature (LCST) behavior.[6–8] If the transition takes place below the critical temperature, it is then designated as an upper critical solution temperature (UCST).[9,10]

This class of "*stimuli-responsive* materials" is very attractive for the development of smart biomaterials, especially for active molecules delivery such as drugs, in cosmetics and also in tissue

engineering. Hydrogels are relevant for their use as scaffolds and as carriers of therapeutic agents such as drugs, cells, proteins and bioactive molecules in the treatment of diseases including dermatological issues, and the repair of tissues.[11–14] For subcutaneous drug delivery, the use of thermosensitive polymers that are soluble at room temperature and form a hydrogel when injected into the body is particularly relevant.[15] For this purpose, thermosensitive polymers and hydrogels could be tuned to display a LCST at physiological body temperature. Moreover, hydrogels could bring several advantages in cosmetic/drug delivery including simplicity of formulation, protective environment for active molecules, prolonged and localized delivery, and ease of application. In the case of tissue engineering such as skin reconstruction, there is a strong interest for hydrogels, especially because their mechanical and biological properties can be tuned to mimic 3D tissue environment and favor reconstruction.[16,17]

In this context, amphiphilic ABA associative copolymers have been developed for the design of smart hydrogels, and the mechanism of hydrogel formation has been thoroughly investigated.[18–20] When ABA triblock copolymers are dissolved into a midblock B selective solvent, A blocks aggregate and drive the formation of micelles in dilute solution, also referred to as "flower micelles".[20,21] When the concentration increases and the micelles start to interact, the A segments can interconnect several micelles, relaxing the entropic constraint associated to the loop formation of the B segments, resulting in the formation of a physically cross-linked 3D hydrogel through bridges. However, these networks can exhibit dangling chains, free chains or loops which do not contribute to the elasticity of the hydrogel. Caused by these defects, ABA systems tend to undergo a broad sol-gel transition at a relatively high concentration ($\geq$ 10 wt%).[22,23]

Since, ABC triblock copolymers have been suggested as interesting alternative to form hydrogels with improved properties.[24] Indeed, this class of copolymers can form hydrogels through

discrete nanodomains promoted by the hydrophobicity of the A and C end-blocks as well as their incompatibility. First contributions in ABC triblock copolymers, have described fluorocarbon and hydrocarbon groups as hydrophobic blocks, resulting in well-segregated hydrophobic domains.[24] Since the A and C blocks are immiscible, the probability to form loops is reduced favoring the formation of bridges.[23] The end-block can also be a thermosensitive polymer such as poly(*N*-isopropyl acrylamide) (PNIPAM), the most investigated thermoresponsive polymer.[25,26] Thermoresponsive ABC triblock-based hydrogels have also been studied with other thermosensitive polymers including poly(2-(dimethylamino)ethyl methacrylate) (PDMAEMA) and poly(di(ethylene glycol) methyl ether methacrylate) (PDEGMMA).[27,28] PNIPAM shows a LCST at ~ 32°C in water which is close to body temperature and tunable by copolymerization with other monomers.[6,8,19] The first report, from Li, C. et *al.* was on a poly(propylene oxide)-*b*-poly(2-methacryloyloxyethyl phosphorylcholine)-*b*-poly(*N*-isopropyl acrylamide) (PPO$_{43}$-*b*-PMPC$_{160}$-*b*-PNIPAM$_{81}$) triblock copolymer which exhibits a sol-gel transition around 37°C at a concentration ≥ 20 wt% with a low mechanical strength (a storage modulus (G') at 25 Pa).[22] Another triblock poly(ethylene-*alt*-propylene)-*b*-poly(ethylene oxide)-*b*-poly(*N*-isopropyl acrylamide) (PON) with block molecular weights of 3-25-10 kDa, elaborated by Lodge group, could form a gel at 5 wt% but the transition occurs at 42°C which is higher than the physiological temperature.[29–32] Derivatives of PON, poly(ethylene-*alt*-propylene)-*b*-poly-(ethylene oxide)-*b*-poly(*N*-isopropyl acrylamide-*co*-acrylic acid) (PEP-*b*-PEO-*b*-P(NIPAM-*co*-AA)) of different molecular weights have also been studied as a double responsive system: pH-sensitive through PAA and temperature-sensitive through PNIPAM, leading to a complex tunable hydrogel.[33] However, these PON-based hydrogels need at least two weeks of preparation through thin-film hydration method. The preparation enables the polymer to form the desired objects in solution that create the 3D network

while heated. A cell protective ABC triblock poly(propylene sulfide)-*b*-(*N*,*N*-dimethyl acrylamide)-*b*-poly(*N*-isopropyl acrylamide) (PPS_{60}-*b*-$PDMA_{150}$-*b*-$PNIPAM_{150}$) has been developed by Gupta et *al.*, showing interesting results by forming stable hydrogel within 30 s at 2.5 wt% between room temperature and body temperature. However, this system presents drawback in terms of mechanical property with G' lower than 1,000 Pa at 7.5 wt% polymer concentration.[34] Moreover, these reported ABC synthetic hydrogels are generally based on non-degradable polymers. Recently, promising hydrogels composed of reactive oxygen species (ROS)-degradable PPS_{135}-*b*-$PDMA_{152}$-*b*-$PNIPAM_{225}$ (PDN), slow hydrolytically degradable PCL_{85}-*b*-$PDMA_{150}$-*b*-$PNIPAAM_{150}$ (CDN, PCL stands for poly(ε-caprolactone)), and fast hydrolytically degradable $PLGA_{60}$-*b*-$PDMA_{148}$-*b*-$PNIPAAM_{152}$ (LGDN – PLGA corresponds to poly(D,L-lactide-*co*-glycolide)) have been developed by the same team and form gels at 5 wt% upon heating to 37°C.[35,36] However, these studies did not report hydrogel morphologies, and rheological measurements show relatively low storage moduli, below 300 Pa.

In the present study, inspired from the work on ABC triblock hydrogels, we have developed a poly(trimethylene carbonate)-*b*-elastin-like polypeptide diblock ($PTMC_{30}$-*b*-MW-($ELP[V_3M_1$-60])-($ELP[I_1$-20])-C(*N*-EtSucc)) ABC triblock copolymer and studied the hydrogel formation. All the blocks were chosen with a rationale and "safety by design" approach. The hydrophobic A block is composed of a synthetic poly(trimethylene carbonate) (PTMC). This polymer is biocompatible but also degrades slowly by surface erosion, mostly by enzymatic hydrolysis, generating non-acidic and non-inflammatory products (1,3-propanediol and carbon dioxide), unlike aliphatic polyesters, making it a great candidate for biomedical applications.[37] As for BC blocks, recombinant elastin-like polypeptides (ELPs) were chosen. ELPs are derived from the hydrophobic domain of tropoelastin and consist of the repeating sequences (-Val-Pro-Gly-Xaa-

Gly-) pentapeptides, where the guest residue Xaa can be any amino acid except proline.[38] This unique class of precision protein-like polymers has *stimuli*-responsive self-assembly properties, exhibiting a reversible sharp lower critical solution temperature, also referred to as inverse transition temperature (denoted Tt).[38,39] ELP chains are entirely soluble in aqueous solution below the Tt; while above the Tt, they phase separate into microparticle-based structures through a coacervation process. This inverse transition temperature can be tuned by modifying macromolecular parameters including the nature of the guest residue Xaa, the molecular weight and concentration of the ELP but also the salinity of the aqueous medium.[40,41] The general trend is that the higher the hydrophobicity of the Xaa residues, the molar mass and the concentration of the ELP in aqueous solution, the lower the Tt.[42] More specifically, as ELPs are derived from elastin, a key protein of the extracellular matrix (ECM) of different connective tissues such as skin, their use could favor the biomimicry of numerous organs' environment.[43–45] Introducing inherently biocompatible ELPs in the triblock system creates a new hybrid bio-inspired hydrogel suitable for tissue engineering.[46,47] Hybrid ELP have already been reported to fabricate hydrogels, combined with poly(ethylene glycol) (PEG).[48–50] However, gels were mostly chemically cross-linked and thus, required chemical cross-linking agents[48,50], often cytotoxic, or required hours of gelation[49]. After synthesis and characterization, the thermoresponsive properties of the ABC triblock copolymer was evaluated by turbidity assays. The morphology of the system was first studied in dilute conditions using dynamic light scattering (DLS) analysis and microscopy techniques such as liquid atomic force microscopy (AFM) and transmission electronic microscopy, at different temperatures. The polymer was then concentrated to form a hydrogel and studied through macroscopic observation and cryogenic-scanning electron microscopy (cryo-SEM). The ABC

triblock behavior was compared to a BC elastin-like diblock polypeptide to understand the morphology of the system in different conditions.

EXPERIMENTAL SECTION

Chemical and materials. Lysogeny Broth (LB) *medium* was purchased from Sigma-Aldrich (France). Yeast extract was obtained from Biokar Diagnostics (France). Ampicillin, glucose and phosphate buffered saline (PBS) 10X were obtained from Euromedex (France). Glycerol and isopropyl β-D-1-thiogalactopyranosi-de (IPTG) were purchased from Fisher Scientific (USA). Toluene was obtained from Fischer Chemical (UK). 1,3-dioxane-2-one (trimethylene carbonate TMC) and 3,5-bis(trifluoromethyl)phenyl isothiocyanate were purchased from TCI Chemicals (Belgium). Benzoic acid, chloroform and sodium bicarbonate were purchased from Acros Organics (Belgium). Cyclohexane, cyclohexylamine, 1,8-diazabicyclo[5.4.0]undec-7-ene (DBU), 4-pentynoic acid, *N*-hydroxysuccinimide (NHS), *N*, *N'*-dicyclohexylcarbodiimide (DCC), sodium azide, copper(II) sulfate pentahydrate, dichloromethane (DCM), ethyl acetate (EtOAc), dimethylsulfoxide (DMSO), magnesium sulfate, petroleum ether and tetrahydrofuran (THF) were purchased from Sigma-Aldrich (France). *N*-ethyldiisopropylamine (DIPEA), dimethylformamide (DMF) and sodium ascorbate were obtained from Alfa Aesar (Germany). [4-(bromomethyl)phenyl]methanol was purchased from ABCR (Germany). Tris(2-carboxyethyl)phosphine hydrochloride (TCEP·HCl) and *N*-ethylmaleimide (NEM) were purchased from TCI Chemicals (Belgium). Ultrapure (UP) water (18 MΩ-cm) was obtained by passing in-house deionized water through a Millipore Milli-Q Biocel A10 purification unit. DMF, THF and toluene were dried by a solvent purification system, before use.

Synthesis of the poly(trimethylene carbonate) A block.

N-cyclohexyl-N′-(3,5-bis(trifluoromethyl)phenyl)thiourea (TU). In a 50 mL round-bottom flask, cyclohexylamine (2.11 mL, 18.4 mmol, 1.0 eq.) was added dropwise at room temperature to a solution of 3,5-bis(trifluoromethyl)phenyl isothiocyanate (3.38 mL, 18.4 mmol, 1.0 eq.) in 16.5 mL of THF. The resulting mixture was stirred at 30°C for 3 h. The reaction was followed by thin-layer chromatography (cyclohexane/EtOAc 2:1): Rf = 0.67 and was then concentrated *in vacuo*. The residue was recrystallized with chloroform to give a white powder (6.39 g, 17.25 mmol, yield: 94 %). ^{1}H nuclear magnetic resonance (NMR) (400.2 MHz, DMSO-d_6, 298K): δ 9.86 (br, 1H, CH-N*H*), 8.23 (s, 2H, 2 C-C*H*=CCF$_3$), 8.16 (br, 1H, C-N*H*), 7.71 (s, 1H, CF$_3$C-C*H*=CCF$_3$), 4.11 (br, 1H, C*H*-NH), 2.01-1.10 (m, 10H, C*H*$_{2\ cyclohexyl}$). ^{13}C NMR (100.7 MHz, DMSO-d_6, 298K): δ 179.1 (*C*=S), 142.0 (=*C*-N), 130.0 (q, J = 30.2 Hz, 2 *C*-CF$_3$), 123.2 (q, J = 271.9 Hz, 2 CF$_3$), 121.8 (2 CF$_3$C=*C*H-C), 115.8 (F$_3$CC=*C*H-CCF$_3$), 52.3 (*C*H-N), 31.6 (2 CH-*C*H$_2$-CH$_2$), 25.1 (CH$_2$-*C*H$_2$-CH$_2$), 24.4 (2*CH$_2$-*C*H$_2$-CH$_2$). Matrix-assisted laser desorption/ionization (MALDI) C$_{15}$H$_{16}$F$_6$N$_2$S: [M+H]$^+$ m/z = 371.12. Melting temperature (T$_m$) = 166.7°C.

[4-(azidomethyl)phenyl]methanol. A mixture of [4-(bromomethyl)phenyl]methanol (1.00 g, 5.0 mmol, 1 eq.), sodium azide (0.50 g, 7.5 mmol, 1.5 eq.) in 55 mL of DMF was stirred under nitrogen for two days. The resulting suspension was poured into water and extracted with dichloromethane. Combined organic layers were dried over magnesium sulfate and evaporated in *vacuum*. The azido-alcohol (ROH) was obtained as an oil (0.56 mg, 3.4 mmol, yield: 69 %). ^{1}H NMR (400.2 MHz, CDCl$_3$, 298K): δ 7.36 (dd, J = 8.0 Hz and 16.0 Hz, 4H, 4 H_{arom}), 4.72 (s, 2H, C*H*$_2$-N$_3$), 4.34 (s, 2H, C*H*$_2$-OH).

General procedure for polymerization of trimethylene carbonate (TMC) in solution. Beforehand, in a flame-dried schlenk, trimethylene carbonate was purified by three successive

recrystallizations in dry ethyl acetate and dried by azeotropic distillation in toluene; 1,8-diazabicyclo[5.4.0]undec-7-ene (DBU) and the alcohol initiator were distillated from CaH_2. In a glovebox, TMC (30 eq.) was dissolved in a flame-dried schlenk by adding toluene to obtained 250 mg/mL. Separately, the initiator ROH (1 eq.) and catalyst system DBU/TU (1.3 eq./1.3 eq.) were dissolved in the same solvent and were then added to the clear, homogeneous solution of monomer. Polymerization was carried out for a given amount of time $t_{polymerization}$ after which an excess of benzoic acid was added to quench the reaction. The polymer was purified by precipitation in cold methanol. The pellet obtained after centrifuge was dried under *vacuum* to give the polymer. *Data* using [4-(azidomethyl)phenyl]methanol as initiator and targeting degree of polymerization (DP) of 30: $t_{polymerization}$= 15 min. Yield = 84 %. ^{1}H NMR (400.2 MHz, CDCl$_3$, 298K): δ 7.36 (dd, J = 8.0 Hz and 16.0 Hz, 4H, 4 H_{arom}), 5.16 (s, 2H, CH_2-N$_3$), 4.35 (s, 2H, CH_2-OH), 4.23 (t, J = 6.0 Hz, 118H, 29.5 CH_2-CH$_2$-CH_2), 3.74 (t, J = 6.0 Hz, 2H, CH_2-OH), 2.05 (quint, J = 6.0 Hz, 58H, 29.5 CH_2-CH$_2$-OC=O), 1.92 (quint, J = 6.0 Hz, 2H, 2 CH_2-CH$_2$-OC=O) (Figure S1).

Synthesis of the elastin-like polypeptide BC blocks.

Based on Chilkoti's nomenclature, the different ELP constructs are distinguished using the notation ELP[XiYj-n], where the bracketed capital letters are the guest residues in the single-letter amino acid code, the corresponding subscripts designate the frequency of each guest residue in the repeat unit, and n describes the total number of pentapeptides repeats.[51]

Construction of the expression vector. By using a variation of the recursive directional ligation method, the sequence coding for MW[VPGVGVPGMG(VPGVG)$_2$]$_{15}$[VPGIG]$_{20}$C was obtained.[52] Briefly, the MW-ELP[V$_3$M$_1$-20] sequence was extracted from the pUC19-MW-ELP[V$_3$M$_1$-20] plasmid by a double digestion with *Bsm*FI and *Btg*ZI, purified by agarose gel electrophoresis,

ligated with the Quick ligation™ kit into the pUC19-MW-ELP[I$_1$-20]-C plasmid that was previously linearized by *Bsm*FI digestion and dephosphorylated.[53] A molar *ratio* 5:1 insert:vector (MW-ELP[V$_3$M$_1$-20]:MW-ELP[I$_1$-20]-C) was used for the ligation step to favor the insertion of multiple MW-ELP[V$_3$M$_1$-20] sequences, and thus obtain MW[VPGVGVPGMG (VPGVG)$_2$]$_{15}$[VPGIG]$_{20}$. After transformation into NEB 5α-F'Iq *E. coli* competent cells, positive clones were identified by colony polymerase chain reaction (PCR) with OneTaq® hot start DNA polymerase and specific primers flanking the insertion site (sense primer: 5'GTGCTGCAAGGCGATTAAGT3'; reverse primer: 5'TGTGGAATTGTGAGCGGATA3'). Clones for which the amplification products were 1380 bp in size, were selected for further experiments. The corresponding plasmids were purified and sequenced. The ELP sequence was then extracted from pUC19-MW-(ELP[V$_3$M$_1$-60])-(ELP[I$_1$-20])-C by a double digestion *Nde*I and *Bam*HI, and ligated with the Quick ligation™ kit into similarly digested and dephosphorylated pET-44a(+) plasmid. The different ligation products were then used to transform BLR(DE3)-competent cells for production. The sequence of the resultant plasmid was confirmed by DNA sequencing. The sequences of the ELP gene and of the corresponding protein are shown in supporting information (Figure S2).

Bioproduction of recombinant ELP. A single bacterial colony was selected and cultured overnight at 37°C on a rotary shaker at 175 rpm in 50 mL of LB *medium* supplemented with 2.5 g/L glycerol and 50 µL of 100 mg/mL ampicillin. The seed culture was inoculated into 1 L rich LB *medium* supplemented with 1 mL of 100 mg/mL ampicillin, and *bacteria* were cultivated at 37°C and 220 rpm in a 5 L flask. When the optical density at 600 nm (OD$_{600}$) reached the value of 0.8, 500 µL of 1M IPTG was added and the temperature of the incubator was decreased to 25°C.

Samples were then collected at several times points for OD_{600} measurement and analyzed by gel electrophoresis (SDS-PAGE) on sodium dodecyl sulfate-polyacrylamide gels (Figure S3).

Isolation and purification of recombinant ELP. After 21 h IPTG-induction, the culture was harvested by centrifugation at 7,500 g and 4°C for 15 min. The cell pellet was resuspended with ultrapure water to target 10 mL/g considering wet weight. The mixture was incubated overnight at − 80°C and defrosted by incubation at 4°C. Cell lysis was completed by sonication at 15°C with sequential 4 s-pulses at 125 W separated by 8 s-resting time periods for a total duration of 45 min. Insoluble debris were removed by centrifugation at 11,000 g and 4°C for 20 min. The cleared lysate was thereafter subjected to three successive rounds of inverse transition cycling (ITC)[39]. The polypeptide was precipitated by increasing temperature at 30°C for 30 min and retrieved by centrifugation at 7,500 g and 30°C for 15 min ("Hot spin"). After removal of soluble proteins in the supernatant, protein-containing pellet was resuspended in cold ultrapure water. Insoluble, heat denatured proteins from *E. coli* were eliminated in the pellet after centrifugation at 7,500 g and 4°C for 15 min ("Cold spin"), while the ELP-containing supernatant was subjected to an additional ITC round. Soluble ELP was then extensively dialyzed against ultrapure water at 4°C using 3 kDa MWCO- dialysis tubing (*Spectra* Por7) and freeze-dried. Beforehand, SDS-PAGE analysis was performed to control the production steps and purification of the ELP (Figure S3). A MW[VPGVGVPGMG(VPGVG)$_2$]$_{15}$[VPGIG]$_{20}$C white fluffy compound was obtained (about 100 mg/L of culture) with a molar mass of 34,001 Da detected by MALDI (Figure S4), containing some dimers formed *via* disulfide bridge between two cysteines (as shown by a double molar mass in Figure S3 last lane, and Figure S4). 1D (^{1}H and ^{13}C) and 2D (HSQC) NMR *spectra* of ELP were recorded in D_2O and carefully assigned (Figure S5).

Cysteine thiol protection: synthesis of MW-(ELP[V$_3$M$_1$-60])-(ELP[I$_1$-20])-C(*N*-EtSucc). In a 10 mL vial containing 100 mg of the diblock (0.003 mmol, 1 eq.), TCEP·HCl (4.22 mg, 0.015 mmol, 5 eq.) was dissolved in 2.5 mL of dry DMF. The solution was flushed 30 min with nitrogen. 7.69 µl of DIPEA (0.044 mmol, 15 eq.) and 2.5 mL of a solution in dry DMF, containing *N*-ethylmaleimide (3.68 mg, 0.03 mmol, 10 eq.) were added to the ELP solution. After 24 hours, the mixture was diluted in ultrapure water, dialyzed against ultrapure water in a 3 kDa dialysis bag, and freeze-dried to give a white fluffy compound (mean yield > 80 %, n = 7, n = number of reactions).

Pent-4-ynoic acid succinimidyl ester. 4-pentynoic acid (2.00 g, 20.38 mmol, 1.00 eq.) was dissolved in 80 mL dry DCM under nitrogen. NHS (2.58 g, 22.42 mmol, 1.10 eq.) and DCC (4.46 g, 21.61 mmol, 1.06 eq.) were added to the solution. The mixture was stirred at room temperature for 3 hours. The precipitated dicyclohexylcarbamide was filtered off with Celite and the filter cake was washed with cold DCM. The filtrate was collected and DCM was removed in *vacuum*. The product was dissolved in EtOAc and cooled at 4°C for 20 minutes. The precipitate was filtered off again with Celite and the filtrate was washed with saturated sodium bicarbonate (x2), brine (x2) and dried over anhydrous MgSO$_4$. It was then filtrated and concentrated in *vacuum* to give a crude product as colorless oil. It was then purified by silica gel column chromatography with petroleum ether:EtOAc 2:1 and the pure product was collected and concentrated to dryness to give a white solid (2.34 g, 11.94 mmol, yield = 58 %). ^{1}H NMR (400.2 MHz, CDCl$_3$, 298K): δ 2.90-2.84 (m, 6H, C*H$_2$*-C*H$_2$* $_{succinimidyl}$ + CH$_2$-C=O), 2.62 (td, 2H, *J* = 2.8 Hz and 8.0 Hz, CH$_2$-C*H$_2$*-C≡), 2.05 (t, *J* = 2.4 Hz, ≡C*H*). T$_m$ = 66.8°C.

Introduction of alkyne group on ELP: synthesis of Alkyne-MW-(ELP[V$_3$M$_1$-60])-(ELP[I$_1$-20])-C(*N*-EtSucc). To a solution of 100 mg of MW-(ELP[V$_3$M$_1$-60])-(ELP[I$_1$-20])-C(*N*-EtSucc)

(0.003 mmol, 1 eq.) in 4.0 mL DMF, pent-4-ynoic acid succinimidyl ester (20.04 mg, 0.103 mmol, 35 eq.) and DIPEA (0.5 µL, 0.003 mmol, 1 eq.) were added. The reaction was stirred at room temperature for 72 hours. Then the mixture was diluted with water and the resulted solution was dialyzed against ultrapure water in a dialysis bag (MWCO 3 500). The final product was obtained by freeze-drying into a white compound (mean yield > 90 %, n = 4).

Synthesis of ABC triblock: PTMC-*b*-MW-(ELP[V₃M₁-60])-(ELP[I₁-20])-C(*N*-EtSucc). The azido-PTMC (6.1 mg, 0.0019 mmol, 1.3 eq.) and Alkyne-MW-(ELP[V₃M₁-60])-(ELP[I-20])-C(*N*-EtSucc) (50.0 mg, 0.0015 mmol, 1.0 eq.) were weighted and dissolved in 500 µl of DMF. Copper(II) sulfate pentahydrate (0.7 mg, 0.0029 mmol, 2.0 eq.) and sodium ascorbate (1.2 mg, 0.0058 mmol, 4.0 eq.) were suspended in 500 µl of DMF. Both solutions were flushed with N_2 for 30 minutes. The reactants solution was transferred in the catalyzer mixture to start the reaction for 24 hours. Cuprisorb was added to complex with copper. A precipitation in diethyl ether was done and after centrifugation, supernatant containing solvents was removed. The pellet was dried and resuspended in cold water. A second centrifugation was done at 4°C to remove the azido-PTMC left. The ELP-containing supernatant was dialyzed against ultrapure water in a dialysis bag (MWCO 3500) and freeze-dried to get a fluffy white compound (35.5 mg, 0.0009 mmol, yield: 50-65 %, n = 2). ^{1}H NMR (400.3 MHz, CDCl₃, 278K): δ 7.75 (s, 1H, $H_{triazole}$), 5.51 (s, 2H, CH_2-N₃), 4.57 (t, 15H, 15 N-CH_{Met}), 4.24 (d, J = 7.2 Hz, 20H, 20 N-CH_{Iso}), 4.17 (d, J = 7.2 Hz, 45H, 45 N-C$H_{Val\ as\ guest\ residue}$), 3.79-3.51 (br, 84H, 80 N-CH_{2Pro} + CH_2-Phenyl + CH_2-OH), 3.70 (t, J = 6.4 Hz, 118H, 29.5 CH_2-CH₂-CH_2), 1.81 (quint, J = 6.8 Hz, 60H, 30 CH_2-CH₂-OC=O) (Figure 1C).

Solution preparation. Hybrid hydrogels were prepared at 10 % w/v by first dissolving the lyophilized PTMC-*b*-MW-(ELP[V₃M₁-60])-(ELP[I₁-20])-C(*N*-EtSucc) in ultrapure water or PBS 1X buffer on ice for several minutes, until a clear, viscous liquid was obtained. For other lower

concentrations, the higher concentration sample was diluted. The sample was then heated to 40°C (controlled by water bath) to form the hydrogel *via* a thermoresponsive structural transition.

Characterization techniques.

Nuclear magnetic resonance (NMR). NMR *spectra* of ELP-containing samples were acquired in D_2O at 278 K on an AVANCE NEO 400 BRUKER spectrometer operating at 400.3 MHz for ^{1}H and equipped with a Bruker multinuclear z-gradient direct cryoprobe-head. NMR *spectra* of other samples either in DMSO-*d6* or in $CDCl_3$ were acquired at 298 K on an AVANCE III HD 400 spectrometer operating at 400.2 MHz and 100.7 MHz for ^{1}H and ^{13}C respectively. The solvent signal was used as the reference signal. *Data* processing was performed using Topspin software. To describe the multiplicities of the signals, the following abbreviations were used: s: singlet, d: doublet, t: triplet, quint: quintuplet, m: multiplet, br: broad. The coupling constants, abbreviated *J*, were expressed in Hz.

Size-exclusion chromatography (SEC). Polymer molar masses and/or dispersities were determined by size exclusion chromatography using dimethylformamide + lithium bromide (LiBr) at 1 g/L as the eluent. Measurements in DMF were performed on an Ultimate 3000 system from Thermoscientific equipped with diode array detector. The system also includes a multi-angle light scattering detector and differential refractive index detector (dRI) from Wyatt technology. Polymers were separated on two KD-803 Shodex gel columns (300 x 8 mm) (exclusion limits from 1000 Da to 50 000 Da) at a flow rate of 0.8 mL/min. Columns temperature was held at 50°C.

Fourier-transform infrared (FTIR). Fourier-transform infrared spectra were acquired at room temperature from 400 to 4000 cm-1 with a Bruker VERTEX 70 spectrometer (resolution: 4 cm-1, 64 scans, DLaTGS MIR) equipped with a Pike GladiATR plate for attenuated total reflectance.

Dynamic scanning calorimetry (DSC). DSC analysis were performed on a TA Instruments RCS under nitrogen and helium at 25 mL/min flow rate. 6 mg samples were weighted and sealed in aluminum pan. Thermograms of three successive cycles were obtained with the following temperature gradients: i) 25°C to 70°C at 10°C/min, ii) 70°C to - 75°C at 10°C/min and iii) - 75°C to 100°C at 10°C/min. It was performed to obtained products specific temperatures including melting temperatures (T_m) and glass transition temperature (T_g).

Sodium dodecyl sulfate-polyacrylamide gel electrophoresis (SDS-PAGE). Electrophoresis were performed using 4-15 % Mini-PROTEIN TGX Stain-Free gel (Bio-Rad) Tris/Glycine/SDS buffer (Bio-Rad). Proteins were dissolved in ultrapure (1 mg/mL) and two-fold diluted with 2x Laemmli sample buffer (Bio-Rad). 15 µl of each solution was then loaded onto the gel. After migration, protein bands were revealed with the Bio-Rad Gel Doc EZ system. In several cases, gels were also stained in contact with Coomassie blue (InstantBlueTM, #ISB1L, Sigma). These gels were also imaged with the Bio-Rad Gel Doc EZ system.

Matrix-assisted laser desorption/ionization (MALDI). Mass spectrometry analysis was performed on a MALDI-ToF-ToF (time of flight) (Ultraflex III, Bruker), which is equipped with a matrix-assisted laser desorption/ionization source. ELP samples were prepared as following: freeze-dried compounds were dissolved in cold water, if soluble, or solubilized in drops of DMSO and diluted in water/methanol (1/1, v/v). Final concentrations vary from 2 to 5 mg/mL. ELP samples were mixed to the matrix solution: sinapinic acid (10 mg/mL in acetonitrile/0.1 % trifluoroacetic acid in water (1/1, v/v)), then, 1-2 µL of this solution were added to a metal plate. After solvent evaporation, the solid residue was exposed under laser (Smartbeam, Nd:YAG, 355 nm). Analysis were performed in positive linear mode, and proteins standards mixture were used for external calibration of the instrument in a mass range adapted to proteins of interest.

Turbidity measurement. Transition temperatures (Tt) were determined by measuring the turbidity at 350 nm between 12 and 80°C at a 1°C/min scan rate at several concentrations (4.7 µM, 9.5 µM, 23.5 µM, 94 µM, 470 µM) in UP water and PBS 1X for MW-(ELP[V_3M_1-60])-(ELP[I_1-20])-C(N-EtSucc) and PTMC$_{30}$-b-MW-(ELP[V_3M_1-60])-(ELP[I_1-20])-C(N-EtSucc). *Data* were collected on a Cary 100 UV–Vis spectrophotometer equipped with a multi-cell thermoelectric temperature controller from Agilent Technologies. The Tt is defined as the highest point of the first derivative curve of absorbance versus temperature.

Dynamic light scattering (DLS). Proteins often tend to collapse on filters and ELPs' Tt depend excessively on concentration. Thus, to avoid any loss of our samples, no filtration has been performed before measurement. Measurements were performed on a Malvern ZetaSizer Nano ZS instrument with detection at 173°. Samples were analyzed at a set up specific temperature. Each result was averaged with three measurements.

Liquid atomic force microscopy (AFM). Liquid AFM imaging in aqueous medium was performed using a Dimension FastScan SPM (Bruker) operated in PeakForce Tapping mode with silicon cantilever (ScanAsyst-Fluid+) with tip radius of 2 nm, a spring constant of 0.7 N/m and a cantilever resonance frequency of about 150 kHz to characterize the surface morphology of polymer solutions. A droplet of each solution was deposited on freshly cleaved highly oriented pyrolytic graphite (HOPG, Ted Pella, grade ZYB), and the morphology of molecules adsorbed on HOPG surface under aqueous medium was observed at 15°C and then at a higher temperature (depending on the transition temperature of the solution) with a controlled thermoelectric cooling system.

Transmission electron microscopy (TEM). TEM images were performed on a Hitachi HT7700 (Tokyo, Japan) with an acceleration voltage at 100 kV. Each sample was dispersed in ultrapure water and a drop of the solution is placed into an ultra-thin carbon film supported on a nickel grid. For cold temperature, the sample was cooled and blotted before measurement, while for higher temperature, the sample was heated at 37°C and blotted before measurement.

Cryogenic-scanning electron microscopy (Cryo-SEM). Cryo-SEM observations were carried out with a JEOL JSM-6700F electron microscope equipped with liquid nitrogen cooled sample preparation and transfer units. A drop of ELP-solution was first set on the specimen holder. For cold ELP-solution, the specimen holder was first cooled before adding sample while for heated ELP-solution, the specimen holder was beforehand heated. The sample was frozen in the slushing station with boiling liquid nitrogen. The specimen was transferred under vacuum from the slushing station to the preparation chamber. The latter was held at T = – 100°C and P = 10-5 mb and was equipped with a blade used to fracture the sample. Once fractured, the sample was coated by a layer of Au–Pd at – 85°C with a chamber pressure that could reach 0.1 mb. For sublimated samples, they were sublimated by increasing temperature up to – 50°C if the solvent is water. It is important to control the vacuum degradation; if it is too fast, the sublimation could be too intense even if – 50 °C is not reached. This process controls the temperature of the frozen sample in vacuum, allowing only the ice formed in the sample to sublimate. Liquid nitrogen was added to stop the process. The sample was then inserted into the observation chamber equipped with a SEM stage cold module held between – 165°C and 180°C, limiting expansion/compression of samples through heat caused by electron beam.

Optical microscopy. ELP optical imaging were performed on an inverted Leica TCS SP5 microscope equipped with an HCX PL APO 63×, NA 1.4 oil immersion objective in bright field

mode. The microscope was equipped with a heating and cooling stage (PE120XY stage size 160*116mm) from Linkam Scientific Instruments, UK, with temperature range: - 25°C to 120°C, heating/cooling rate: 0.1 to 20°C/min, and control and stability: +/- 0.1°C. 10 µl of each solution were injected into a semi-enclosed imaging spacer, sealed by a cover slip to prevent evaporation. The prepared sample slide was then installed immediately on the temperature pad. The starting temperature for all samples was 4°C. A rate of 10°C/min for increasing and decreasing temperature were employed for each sample. The laser power was set up at 3 % while the line average and the gain for bright field at 8 and 362, respectively.

RESULTS AND DISCUSSION

Synthesis of PTMC$_{30}$-b-MW-(ELP[V$_3$M$_1$-60])-(ELP[I$_1$-20])-C(N-EtSucc) ABC triblock. The hybrid PTMC$_{30}$-b-MW-(ELP[V$_3$M$_1$-60])-(ELP[I$_1$-20])-C(N-EtSucc) triblock copolymer was synthesized in several steps. The A block corresponding to poly(trimethylene carbonate) (PTMC) was synthesized by ring opening polymerization (ROP) of trimethylene carbonate (TMC) using an organic catalysis approach.[54] To control the polymerization and avoid transcarbonatation side-reactions (Figure S6), a thiourea/amine catalyst system that works through a dual activation mechanism was used. The monomer was activated by the thiourea to become more electrophilic while the alcohol initiator was activated by the tertiary amine 1,8-diazabicyclo(5.4.0)undec-7-ene (DBU) to become more nucleophilic (Figure S7). The crystalline thiourea N-cyclohexyl-N'-(3,5bis(trifluoromethyl) phenyl)thiourea (TU) was successfully obtained by the reaction between 3,5-bis(trifluoromethyl)phenyl isothiocyanate and cyclohexylamine[55–57], as assessed by ^{1}H and ^{13}C nuclear magnetic resonance (NMR) analyses (Figure S8). The use of organo-catalysts increased

the rate of the ROP ($t_{polymerization}$ = 15 min) while still yielding a polymer with a narrow dispersity (Đ = 1.01) (Figure S1A, B) and a degree of polymerization DP = 30.

The size exclusion chromatography (SEC) traces were perfectly symmetric, attesting the control of the polymerization reaction and the absence of side reactions, especially transcarbonatation reactions. The initiator used was [4-(azidomethyl)phenyl] methanol, obtained from the commercially available [4-(bromomethyl) phenyl]methanol, in order to introduce an azide group necessary for subsequent coupling with the BC block by copper-catalyzed azide-alkyne click cycloaddition (CuAAc) reaction.[58] The characteristic resonance peak of phenyl protons, in addition to the resonance peak corresponding to the CH_2 adjacent to the azide group, were used to determine the 100 % polymerization conversion *via* ^{1}H NMR analysis (Figure S1C). The Fourier-transform infrared (FTIR) *spectrum* (Figure S9) also evidenced the presence of the azide group with a characteristic peak at 2101 cm^{-1}. The PTMC synthesized with a degree of polymerization DP = 30 presents a semi-crystalline character as revealed differential scanning calorimetry (DSC) analysis (Figure S10), with a T_m = 37.6°C and a T_g = - 22.2°C. However, the recrystallization seemed really slow as the transition could only be observed during the first cycle, in agreement with previous contributions.[59]

The BC blocks was obtained from the diblock made of ELPs: MW-(ELP[V_3M_1-60])-(ELP[I_1-20])-C which is composed of a *N*-terminal methionine and valine-containing block (ELP[V_3M_1-60]) and a *C*-terminal-isoleucine containing block (ELP[I_1-20]). ELP[V_3M_1-60] consists of 15 repeats of the sequence [VPGVG-VPGMG-(VPGVG)$_2$], while ELP[I_1-20] corresponds to 20 repeats of the (VPGIG) pentapeptide containing solely isoleucine as the guest residue. ELP[V_3M_1-60] was chosen as the B block as it presents a significant length to favor bridging at low concentration during hydrogel formation. Methionine residues in this block could also be explored

to introduce specific functionalities (such as cell adhesion sequences, hydrophilic moieties, *etc*.) by chemoselective post-modifications.[60–62] ELP[I_1-20] with hydrophobic isoleucine residues shows an inverse transition below physiological temperature at any concentration (26.2°C at 10 µM in PBS).[53] With a Tt well below 37°C, this block shall act as the C thermosensitive block to form hydrogels in physiological conditions. A cysteine residue was placed at the *C-terminus* for potential introduction of specific moieties (*e.g.*, dyes) or dimerization *via* disulfide bridges. A short leader sequence consisting in methionine and tryptophan residues at the *N-terminus* of the ELP sequence was introduced for proper initiation of translation in *E. coli* and ultraviolet-visible (UV-Vis) detection purposes, respectively. This ELP was produced in *Escherichia coli (E. coli)* using recombinant DNA and protein-engineering techniques. For this, a synthetic gene encoding the following amino acid sequence (Figure S2): MW[VPGVG-VPGMG-(VPGVG)$_2$]$_{15}$[VPGIG]$_{20}$C was constructed by recursive directional ligation of the gene for (ELP[V_3M_1-20]) after a first ligation with the gene of (ELP[I_1-20])-C. After cloning of the ELP-encoding gene, the protein polymer was expressed in *E. coli*, extracted from cell lysates and purified by inverse transition cycling (ITC) avoiding the use of time-consuming and expensive chromatography purification techniques.[39] The purity of the ELP fraction was assessed by sodium dodecyl sulfate-polyacrylamide gel electrophoresis (SDS-PAGE) (Figure S3), and the sample was then dialyzed extensively against ultrapure water before freeze-drying, providing a pure ELP. The yield of purified ELP was around 100 mg/L culture (corresponding to 2.9 µmol/L). The molecular mass of MW-(ELP[V_3M_1-60])-(ELP[I_1-20])-C was determined using matrix-assisted laser desorption/ionization (MALDI) mass spectrometry, and found to be in agreement with the theoretical value of 33,958.8 Da (Figure S4). Either on the last lane of the SDS-PAGE or on the mass *spectrum*, a trace and a peak, respectively at double mass appeared, that could correspond to
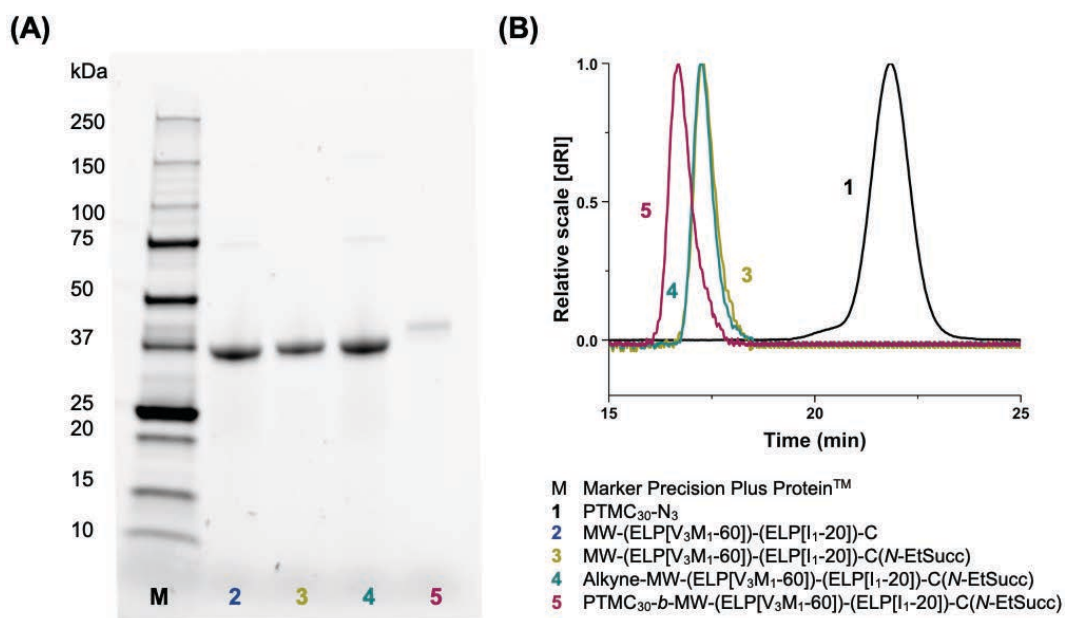
a MW-(ELP[V_3M_1-60])-(ELP[I_1-20])-C-C-(ELP[I_1-20])-(ELP[V_3M_1-60])-WM formed by two MW-(ELP[V_3M_1-60])-(ELP[I_1-20])-C *via* intermolecular disulfide-bridge formation. MW-(ELP[V_3M_1-60])-(ELP[I_1-20])-C was also characterized by 1D- and 2D-NMR analyses (Figure S5).

The *N*-terminal cysteine was subsequently modified to avoid disulfide bridge formation. TCEP·HCl was added to the solution to reduce the S-S bonds. *N*-ethylmaleimide (NEM) was introduced by Michael addition reaction in basic conditions with *N*-ethyldiisopropylamine (DIPEA). After extensive dialysis against ultrapure water and freeze-drying, the isolated product, MW-(ELP[V_3M_1-60])-(ELP[I_1-20])-C(*N*-EtSucc), was characterized by SDS-PAGE (Figure 1A - Lane 2 compared to lane 1) and SEC in DMF (Figure S11). Full reduction of disulfide bridges and absence of dimers were confirmed by these analyses.

Finally, an alkyne function was introduced at the *N*-terminal end for subsequent conjugation with the A block by CuAAc. For this, a commercially available 4-pentynoic acid was first modified with *N*-hydroxysuccinimide (NHS) to obtain pent-4-ynoic acid succinimidyl ester, *via* an esterification reaction using a coupling reagent 1,3-dicyclohexylcarbodiimide (DCC) as coupling reagent.[63] The pent-4-ynoic acid succinimidyl ester was then involved in an acylation reaction with the terminal amino group of the MW-(ELP[V_3M_1-60])-(ELP[I_1-20])-C(*N*-EtSucc). The product was analyzed by SDS-PAGE (Figure 1A - Lane 3 compared to lane 2). A faint additional band was observed above 75 kDa, that was attributed to non-covalent interactions between different ELP chains that were resistant to the denaturing conditions used.

With both azido-functionalized A and alkyne-terminated BC blocks in hand, the ABC triblock was obtained by CuAAc using a mixture of copper (II) sulfate and sodium ascorbate in DMF, with

an excess of the $PTMC_{30}-N_3$. After 24 hours of reaction, purification started with a precipitation in diethyl ether to remove the solvent. The product was then resuspended in cold water and a second centrifugation was performed at 4°C to remove the azido-PTMC left and give the triblock ABC. The triblock formation was assessed by SDS-PAGE (Figure 1A –Lane 4 compared to lane 3) and SEC in DMF (Figure 1B) where a significant shift to higher molecular weight was observed. The formation of the triazole function was confirmed by the appearance of a characteristic resonance peak at $\delta = 7.5$ ppm integrating for one proton on the ^{1}H NMR *spectrum* (Figure 1C).

M   Marker Precision Plus Protein™
1   $PTMC_{30}-N_3$
2   MW-(ELP[V_3M_1-60])-(ELP[I_1-20])-C
3   MW-(ELP[V_3M_1-60])-(ELP[I_1-20])-C(*N*-EtSucc)
4   Alkyne-MW-(ELP[V_3M_1-60])-(ELP[I_1-20])-C(*N*-EtSucc)
5   $PTMC_{30}$-*b*-MW-(ELP[V_3M_1-60])-(ELP[I_1-20])-C(*N*-EtSucc)

(C)
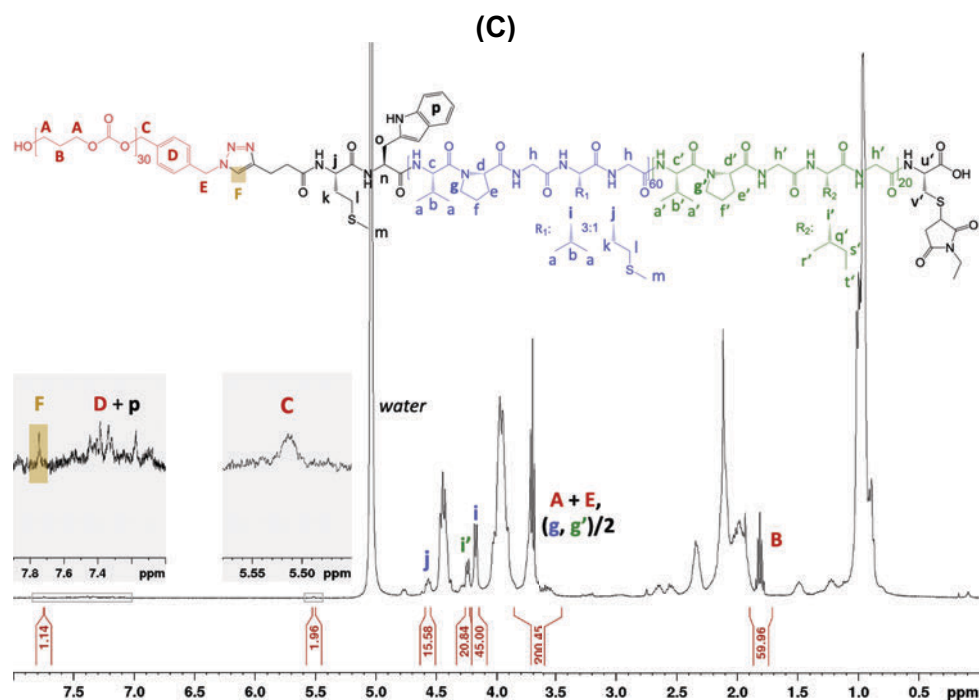
Figure 1. ABC triblock characterization. **(A)** SDS-PAGE (stain-free gel) of elastin-like polypeptides derivatives. Precision Plus Protein™ unstained standards (Bio-Rad) were used as molecular weight markers. **(B)** SEC dRI detection of – PTMC$_{30}$, – MW-(ELP[V$_3$M$_1$-60])-(ELP[I$_1$-20])-C(*N*-EtSucc), – Alkyne-MW-(ELP[V$_3$M$_1$-60])-(ELP[I$_1$-20])-C(*N*-EtSucc), – PTMC$_{30}$-*b*-MW-(ELP[V$_3$M$_1$-60])-(ELP[I$_1$-20])-C(*N*-EtSucc) in DMF + 1 g/L LiBr. **(C)** ^{1}H NMR *spectrum* of PTMC$_{30}$-*b*-MW-(ELP[V$_3$M$_1$-60])-(ELP[I$_1$-20])-C(*N*-EtSucc) in D$_2$O at 278 K.

The characteristics, such as molecular weight, dispersity Đ and reactions yield, of the ABC triblock and synthetic intermediates are summarized in Table 1.

Table 1. ABC triblock characterization: mass M, dispersity Đ and reaction yield.

Product (N°)	Name	M^a (g/mol)	Đ^b	Yield (%)
1	PTMC$_{30}$-N$_3$	3689.81	1.01	84
2	MW-(ELP[V$_3$M$_1$-60])-(ELP[I$_1$-20])-C	33958.36	*	100 mg/L
3	MW-(ELP[V$_3$M$_1$-60])-(ELP[I$_1$-20])-C(*N*-EtSucc)	34083.49	1.01	> 80
4	Alkyne-MW-(ELP[V$_3$M$_1$-60])-(ELP[I$_1$-20])-C(*N*-EtSucc)	34163.57	1.01	> 90
5	PTMC$_{30}$-*b*-(ELP[V$_3$M$_1$-60])-(ELP[I$_1$-20])-C(*N*-EtSucc)	37853.38	1.01	50

^{a}Determined using mass spectroscopy. ^{b}Determined using size exclusion chromatography in *N*,*N*-dimethylformamide.
*Two populations: MW-(ELP[V$_3$M$_1$-60])-(ELP[I$_1$-20])-C and its dimer.

The hybrid PTMC$_{30}$-b-MW-(ELP[V$_3$M$_1$-60])-(ELP[I$_1$-20])-C(N-EtSucc) triblock was therefore synthesized through two chemoselective modifications of the recombinant diblock ELP, MW-(ELP[V$_3$M$_1$-60])-(ELP[I$_1$-20])-C followed by a final coupling with PTMC-N$_3$. The yields indicated in Table 1 have been averaged over 4 different runs. Considering the 3 main reactions starting from the pristine recombinant ELP, an overall yield of 36 % was obtained. While the CuAAc reaction was quantitative, this relative low yield was due to mass losses during triblock purification.

The ABC triblock copolymer was successfully obtained through chemoselective modification of elastin-like polypeptides diblock, demonstrating the interest of using recombinant ELP. The N-end as well as the C-terminal cysteine residue of the polypeptide have been modified, but other functionalities could also be introduced onto the thioether group of methionine, offering another opportunity to further tune ELP properties.[60–62] It is important to note that the triblock of this study, has been synthesized solely for academic purposes to evaluate and understand its physico-chemical behavior without any industrial development objective since the synthesis strategy does not meet L'OREAL's green chemistry *criteria*.

PTMC-b-(ELP[V$_3$M$_1$-60])-(ELP[I$_1$-20])-C(N-EtSucc) triblock thermal properties.

The influence on the transition temperatures (Tts) of the ABC triblock due to the introduction of the synthetic PTMC polymer was evaluated and compared with the Tts of the diblock MW-(ELP[V$_3$M$_1$-60])-(ELP[I$_1$-20])-C(N-EtSucc). For this, cloud point measurements were performed by UV-Vis spectroscopy in ultrapure (UP) water and in PBS at different concentrations to determine Tt values (Figure S12, Table S1). Depending on sample concentration, the Tt of MW-(ELP[V$_3$M$_1$-60])-(ELP[I$_1$-20])-C(N-EtSucc) ranged from 22°C (470 μM) to 28°C (4.7 μM) in UP

water, and from 19°C (470 µM) to 26°C (4.7 µM) in PBS. Concerning the triblock, Tt ranged from 21°C (235 µM) to 33°C (4.7 µM) in UP water. In PBS, two transitions could be seen: from 20°C (235 µM) to 22°C (4.7 µM) [Transition 1] and from 25°C (235 µM) to 28°C (4.7 µM) [Transition 2].

From these results, we emphasized different characteristics of our system. Surprisingly, a unique transition temperature was observed for the diblock ELP while both blocks should exhibit separate transition temperatures as would be expected from a previous work.[64] In addition, for both the diblock and the triblock, the Tt value was inversely correlated to the ELP concentration, in agreement with previously reported contributions, especially from Meyer et *al*.[40] It is also noticeable that the higher the concentration, the higher the turbidity of the solution at low temperature (Figure S12). In the case of the diblock, the presence of aggregates, increasing with concentration of the solution may explain this phenomenon. In the case of the triblock, with a hydrophobic A block and BC solvated blocks, this phenomenon was even more pronounced. This can be easily explained by the amphiphilic character of the triblock, resulting in their self-assembly in micellar structures. Furthermore, Tts were lower in PBS than in UP water for both diblock and triblock copolymers. Indeed, the presence of salts accentuated protein aggregations leading to lower the transition temperature of the solution in PBS.[41] This also explained the higher absorbance at low temperature for a given ELP concentration in PBS buffer compared to UP water.

Finally, the Tt values experimentally determined for diblock and triblock copolymer solutions were plotted as a function of concentration in a semi-log plot (Figure 2). The linear dependency of this representation fitted well the empirical model developed by the Chilkoti group[40]:

$$T_t = T_{t,c} + \frac{k}{L} \ln \left(\frac{c_c}{c} \right)$$

with $T_{t,c}$ (°C), the critical temperature, C_c (μM), the critical concentration, k a constant (°C) and L the number of pentapeptides.
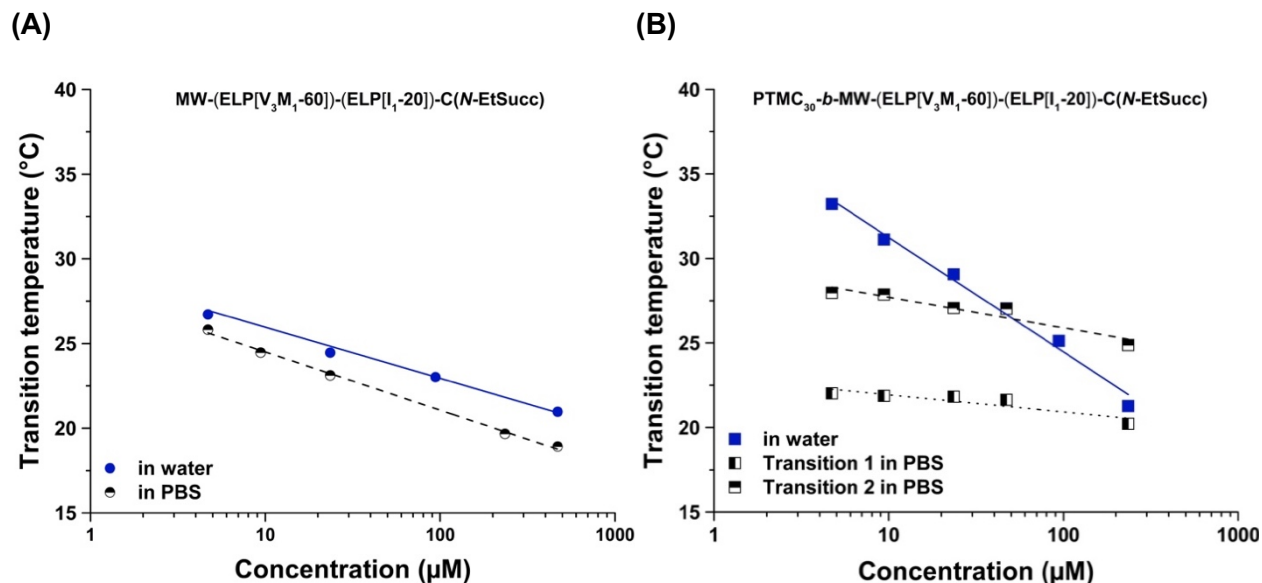
(A)   **(B)**

Figure 2. Tt values of MW-(ELP[V_3M_1-60])-(ELP[I_1-20])-C(N-EtSucc) **(A)** and PTMC$_{30}$-b-MW-(ELP[V_3M_1-60])-(ELP[I_1-20])-C(N-EtSucc) **(B)** plotted as functions of sample concentration in UP water. The lines represented the fit according to Chilkoti's model.

Figure 2 showed the expected tendency: the higher the concentration, the lower the transition temperature. In addition, only one transition was observed in UP water for both diblock and triblock systems. ABC triblock revealed a stronger dependency of Tt *vs* concentration as compared with the diblock. PTMC might accelerates particles' aggregation due to its hydrophobicity. Interestingly, in PBS, ABC triblock solutions showed two transitions (Figure 2B, S12E). First, as mentioned above, the salinity of PBS led to an increase in aggregation, and thus conversely, in a decrease of the transition temperature. Then, the presence of PTMC on the ELP diblock generated the formation of micelles (as assessed by dynamic light scattering), which implies an increase of the ELP local concentration. This could favor the resurgence of two transition temperatures

specific to each ELP block and the lowering of the transition temperature, especially visible in PBS. The reversibility of the phase transition process of ELP was evaluated for the diblock BC and the triblock ABC. Figure 3 corresponds to turbidity analysis through three steps: heating, cooling, 2nd heating for the diblock and for the triblock at 25 µM in UP water and PBS.
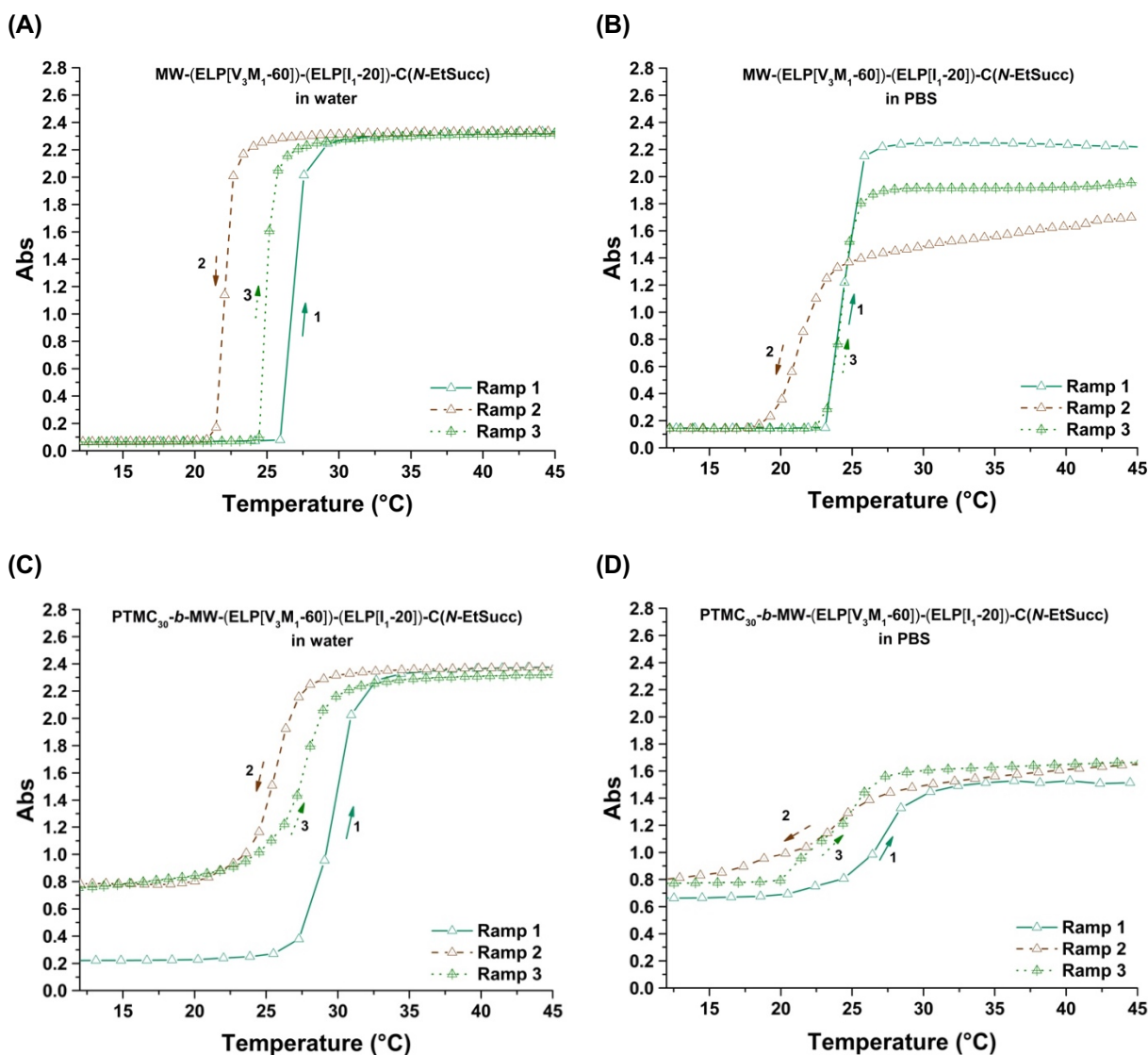

Figure 3. Turbidity assays of the diblock BC at 25 µM in UP water **(A)** and in PBS **(B)**, and of the triblock at 25 µM in UP water **(C)** and in PBS **(D)** through three ramps of temperature: 1. heating, 2. cooling, 3. 2nd heating.

In UP water solution (Figure 3A, C), the diblock copolymer presented a low absorbance level at temperature below Tt, consistent with the presence of freely soluble polymer chains. When cooling, a typical hysteresis of the transition was normally observed. However, the second heating run showed a shift to a lower temperature that might be due to some irreversible aggregation from the previous heating step. The triblock copolymer formed micelles at low temperature, the absorbance being already at 0.2, and these micelles associated when increasing the temperature. When cooling, aggregates did not dissociate explaining the higher absorbance at 0.8 below Tt.

In the presence of PBS (Figure 3B, D), shifts in the maximal absorbance at high temperature after the different temperature cycles could be observed. For the diblock, a decrease in the maximal absorbance values measured at the beginning of the first cooling ramp and at the end of the second heating ramp occurred, compared to the values at the end of the first heating ramp. This may be due to a small amount of aggregates that irreversibly sedimented at the bottom of the cuvette, thereby decreasing the concentration of the sample. However, this decrease in concentration should be limited as we measured the same Tt for the two heating ramps. For the triblock in PBS, we observed a slight increase in the maximal absorbance during the experiment. This may suggest that the aggregates formed at a temperature above Tt became more difficult to dissociate as the incubation time at 45°C increased.

In order to provide a better understanding of the system mechanism, additional experiments were needed, especially using scattering and microscopy experiments.

PTMC-*b*-(ELP[V$_3$M$_1$-60])-(ELP[I$_1$-20])-C(*N*-EtSucc) triblock in dilute and semi-dilute conditions. Before studying the gelation process of the triblock that occurred at high

concentration, the system was studied at relatively low concentration to understand the mechanism of self-assembly. The solutions were further studied by light scattering along with microscopy observations.

Dynamic light scattering (DLS) was first used to estimate the sizes of the particles formed by the diblock and the triblock below and above their transition temperatures at different concentrations in UP water (Figure 4 and S13, S14). The average scattering intensity of the different polymer solutions was also determined *via* the so-called derived count rate (DCR), which roughly correspond to the number of photons detected. The scattered intensity (or DCR) values were then be compared between samples: an increase of particle size and/or concentration both contributed to a larger DCR value.
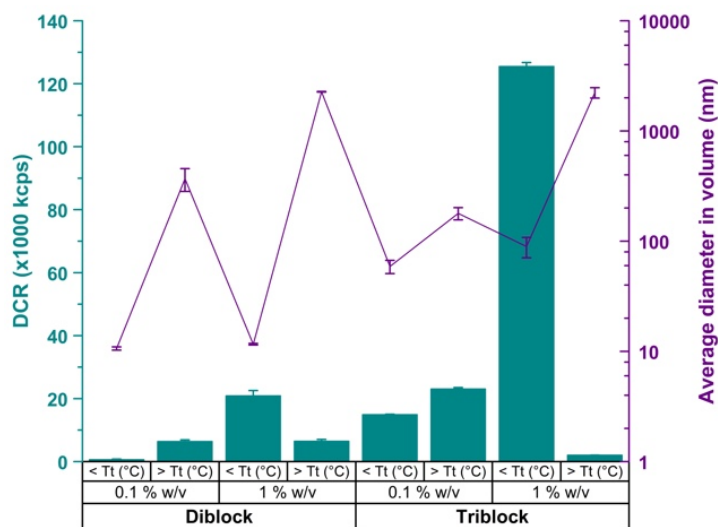
Figure 4. Evolution of the derived count rate (DCR), the average diameter in volume as functions of temperature at a 173° scattering angle for diblock and triblock at 0.1 and 1 % w/v in UP water.

The ELP diblock solution at 0.1 % w/v (29 µM) in UP water showed a DCR close to 500 kcps at low temperature, which is extremely low, meaning that it was mainly soluble. When the

temperature was increased above the Tt, DCR was raised up to 6500 kcps with a size in diameter estimated at 370 nm. Thus, above Tt, several hundred nanometer-sized particles were formed. This is consistent with turbidity assays where the absorbance was higher above the Tt. When increasing concentration at 1 % w/v (293 µM), DCR at low temperature was larger than for a solution at 0.1 % w/v. Indeed, both, the increase in concentration and the possible presence of few aggregates in the solution would contribute to such an increase. Above its Tt, DCR decreased while the size of the formed particles increased, up to several micron-size, consistent with a sedimentation of particles.

Concerning the ELP triblock, its solution at 0.1 % w/v (26 µM) in UP water already showed a relatively high DCR at low temperature. This is perfectly consistent with the formation of micelles with a measured size around 60 nm, in good agreement with previous turbidimetry results. When the temperature was increased above Tt at 30°C, DCR and particle size also increased to approximately 100 nm with several aggregates as shown in Figure S13D. While the concentration was raised to 1 % w/v (264 µM), at low temperature, 80-90 nm micelles were present. By increasing temperature to 30°C, the triblock aggregated and precipitated, as deduced from the increase in size and the decrease in DCR.

Atomic force microscopy (AFM) in liquid phase was performed on both diblock and triblock at 0.1 % w/v (29 µM and 26 µM, respectively) to directly visualize their morphology in dilute conditions (Figure 5).
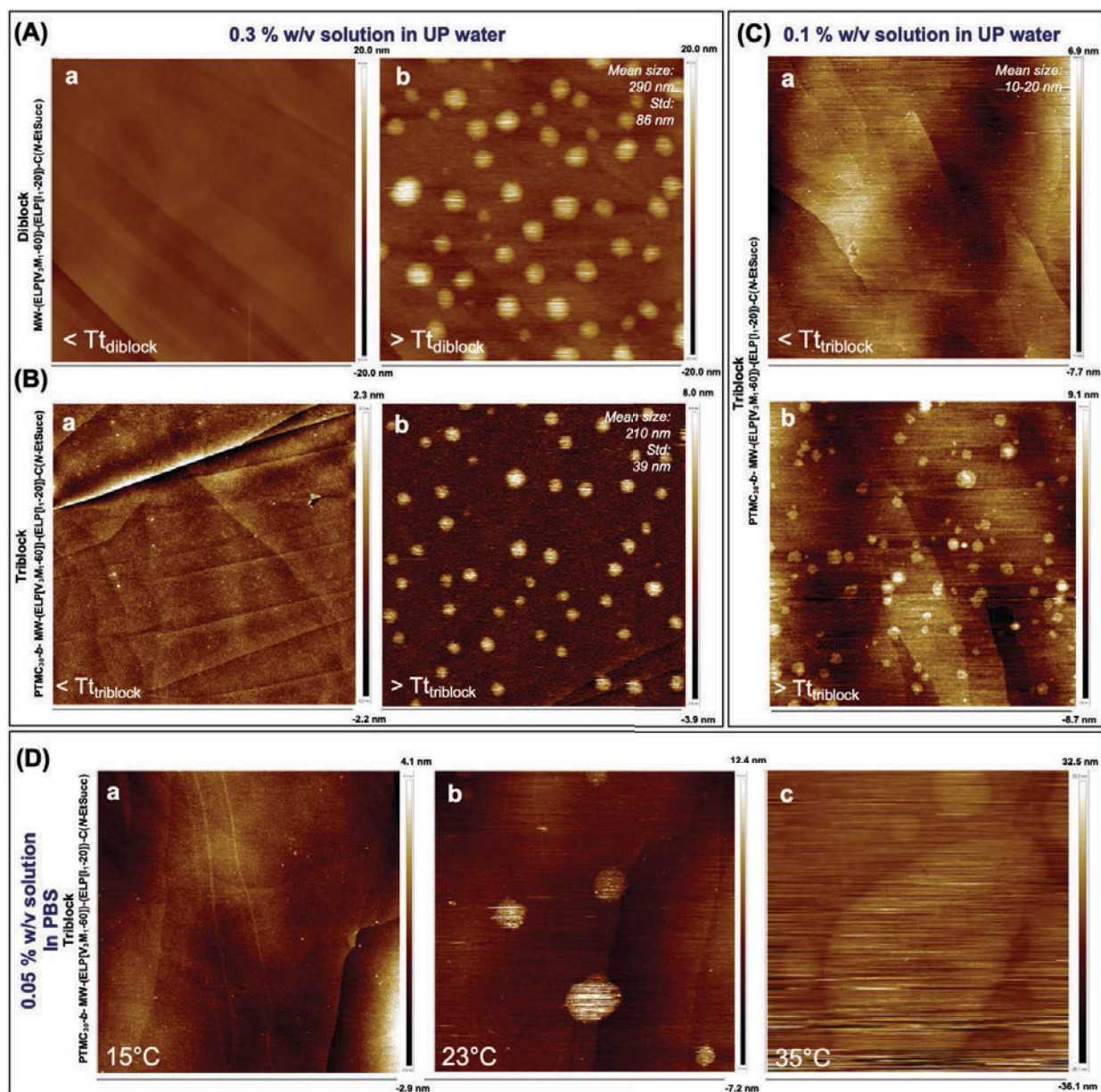
Figure 5. Liquid AFM images. **(A)** MW-(ELP[V_3M_1-60])-(ELP[I_1-20])-C(*N*-EtSucc) solution in UP water at 0.3 % w/v, (a) cooled at T < Tt$_{diblock}$ and (b) heated at T > Tt$_{diblock}$. **(B)** PTMC$_{30}$-*b*-MW-(ELP[V_3M_1-60])-(ELP[I_1-20])-C(*N*-EtSucc) solution in UP water at 0.3 % w/v, (a) cooled at T < Tt$_{triblock}$ and (b) heated at T > Tt$_{triblock}$. **(C)** PTMC$_{30}$-*b*-MW-(ELP[V_3M_1-60])-(ELP[I_1-20])-C(*N*-EtSucc) solution in UP water at 0.1 % w/v, (a) cooled at T < Tt$_{triblock}$ and (b) heated at T > Tt$_{triblock}$. **(D)** PTMC$_{30}$-*b*-MW-(ELP[V_3M_1-60])-(ELP[I_1-20])-C(*N*-EtSucc) solution in PBS at 0.05 % w/v, (a) cooled at 15°C (T < Tt$_{1\ triblock}$), (b) heated at 23°C (Tt$_{1\ triblock}$ < T < Tt$_{2\ triblock}$) and (c) heated at 35°C (T > Tt$_{2\ triblock}$). Images size: 5 µm.

For the diblock (Figure 5A), below its Tt, no object was visible, consistent with the presence of free chains in solutions. When temperature was raised above Tt, coacervates could be observed through a liquid-liquid phase transition, resulting in approximately 300 nm diameter particles, a result in good agreement with the DLS measurements. For the triblock copolymer (Figure 5B), below its Tt, we observed particles of approximately 30 nm in diameter, corresponding to micelles with a PTMC core and an ELP shell. Above the Tt, aggregation of these small micelles occurred which is clearly visible for a concentration of 0.3 % w/v (Figure 5C). This phenomenon was fully reversible as shown in Figure S14. Again, all these observations correlated well with DLS results. Liquid AFM images of the triblock in PBS have also been performed at 0.1 % w/v but unfortunately, after the first transition temperature (21.5°C), the solution was too turbid to provide any good image. Consequently, experiments have been completed at 0.05 % w/v and at 15°C (Figure 5D). At low temperature, 30 nm diameter particles were observed, in agreement with the experiments performed in UP water. At 23°C (after the first Tt), approximately 1 µm-size particles were formed, and turned into 3-4-micron spherical objects at 35°C (after the second Tt). As shown, the triblock solution in PBS solution exhibited two transitions, confirming data from the turbidity assays. The presence of PTMC on ELP diblock generated micelles formation which increased the local concentration of ELP, especially in PBS, favoring the resurgence of the transition temperature of the two separate ELP blocks. Transmission electron microscopy (TEM) experiments confirmed all these observations (Figure S15).

PTMC-*b*-(ELP[V$_3$M$_1$-60])-(ELP[I$_1$-20])-C(*N*-EtSucc) triblock at high concentration.

As shown in Figure 6, a 0.1 % w/v sample of the PTMC-*b*-(ELP[V$_3$M$_1$-60])-(ELP[I$_1$-20])-C(*N*-EtSucc) triblock resulted in a transparent liquid at 5°C that became slightly turbid and bluish when heated to 40°C.
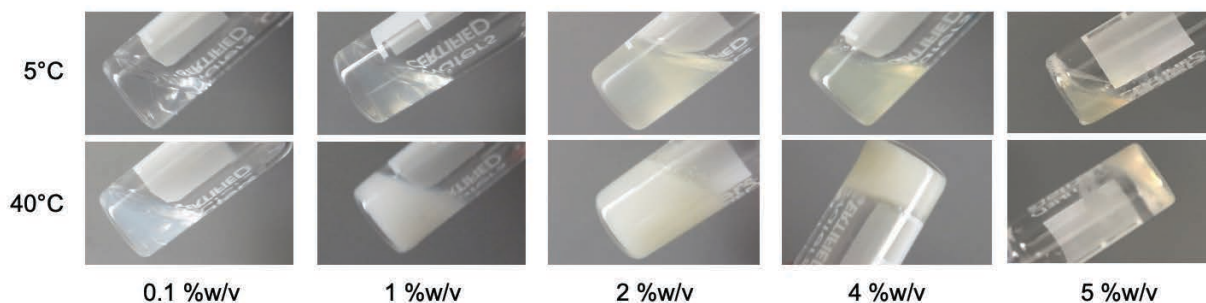
Figure 6. Photographs of PTMC$_{30}$-*b*-MW-(ELP[V$_3$M$_1$-60])-(ELP[I$_1$-20])-C(*N*-EtSucc) solutions at varying triblock concentrations and the indicated temperatures in UP water.

When increasing concentration while remaining at low temperature, the turbidity increased along with the micelle's concentration. At 40°C, the triblock solution was a viscous liquid from 1 % w/v to 2 % w/v, and became a free-standing hydrogel at 4 % w/v. However, at 5 % w/v, the free-standing hydrogel underwent syneresis. Like many PNIPAM-based hydrogels[65,66], the formed hydrogel contracted spontaneously and irreversibly, associated with the expulsion of water. This was eventually promoted by the tendency of hydrogels to exude water that can occur when the equilibrium solvent/macromolecules is not fulfilled, disturbing the network.[67]

Cryo-SEM on the 4 % w/v sample without sublimation was first performed to observe the morphology of these hydrogels (Figure 7A, B). As shown on Figures 7A$_1$ and A$_2$, the sample prepared at low temperature revealed the presence of nano-size particles while at high temperature (Figure 7B), interconnected micron-size spheres were formed. Sublimation of the sample at 4 % w/v and at 8 %w/v revealed a decrease in pore size while increasing concentration (Figure S16A, B). This decrease could explain the shrinking of the hydrogel by a release of water.
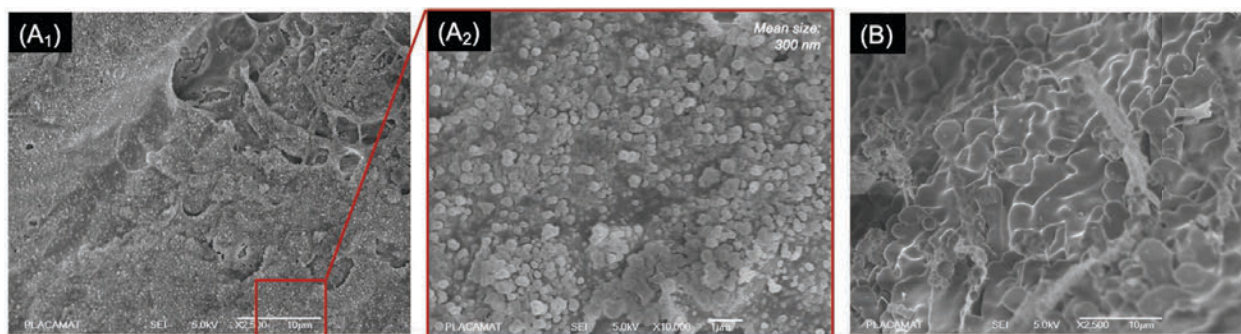
Figure 7. Cryo-SEM images of non-sublimated $PTMC_{30}$-*b*-MW-(ELP[V_3M_1-60])-(ELP[I_1-20])-C(*N*-EtSucc) solution in UP water at 4 % w/v: **(A)** at low temperature [(A$_2$) corresponds to the enlarged image of the area highlighted in red on the image (A$_1$) - Scale bar = 1 µm], and **(B)** at high temperature. Scale bar = 10 µm.

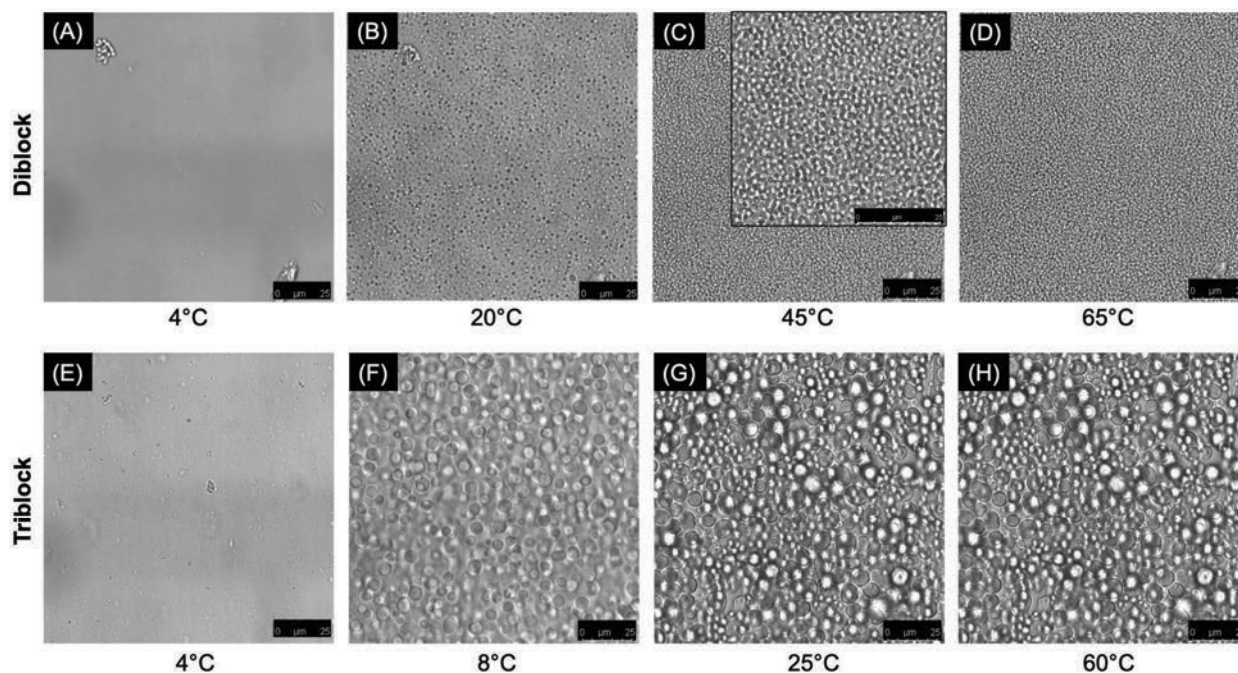Optical imaging has also been performed for diblock and triblock solutions at 5 % w/v in UP water (Figure 8).

Figure 8. Optical images in bright field of the diblock **(A-D)** and triblock **(E-H)** solutions at 5 % w/v in UP water images, at different temperatures, stabilized during 3 minutes. Scale bar = 25 µm. (Video S1 and S2).

It is important to notice that this technique could only measure objects in the micron-size range. Either for the diblock or the triblock, at low temperature (Figure 8A, E), there were no observable object in these conditions, consistent with previous results: the diblock was soluble at low temperature while in the case of triblock, nano-size objects were formed.

While heating above their Tts, two different assemblies occurred for the diblock and triblock solutions, respectively. In the case of ELP diblock, about 2 µm size coacervates formed and stayed stable with time, and during temperature increase (Figure 8B, C, D). The ELP triblock displayed some merging between micron-size particles, already at 8°C (Figure 8F), until 25°C was reached. The micron spheres tended to coalesce showing larger droplets where spheres seemed to stabilize overtime (Figure 8G) even after increasing temperature (Figure 8H).

CONCLUSION

The different analysis performed to evaluate ABC triblock behaviour in diluted and concentrated systems enabled us to propose hydrogels formation mechanism depicted in Figure 9 ~~Figure 12~~.
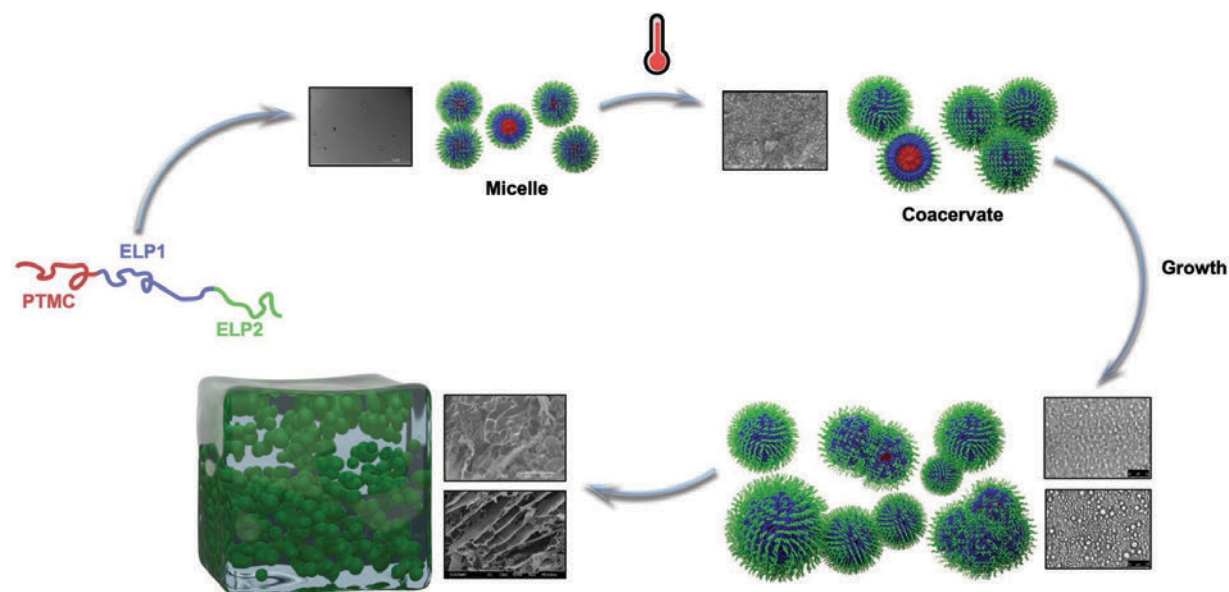

Figure 9. Representative scheme of triblock ABC hydrogel formation (not to scale). **1**. Micelles at low temperature (TEM Image from Figure S15C); **2**. Several hundred nano-size particles while above Tt (Cryo-SEM image from Figure 7B); **3**. Merging nanoparticles into micro-size spheres (Optical image from Figure 8F); **4**. Coalescing globules allowing to form 3D network with pores (Optical image from Figure 8G-H and Cryo-MEB from Figure S16).

The investigation of the ABC triblock composed of $PTMC_{30}$-b-MW-$(ELP[V_3M_1$-$60])$-$(ELP[I_1$-$20])$-C(N-EtSucc) with a hydrophobic A block, a hydrophilic B block and a C hydrophobic and thermosensitive block, demonstrated the versatility of these ELPs. Indeed, we have validated the potential of chain-ends and cysteine bioorthogonal conjugation of ELP leading to the synthesis of an almost monodisperse hybrid triblock (Đ = 1.01). Unlike conventional triblock ABC mentioned in the introduction, we have shown a different mechanism for the formation of hydrogels. Indeed,

through the study of the triblock in dilute and concentrated solution, we managed to suggest a consistent mechanism of formation as described in Figure 9. It consists of the formation of microspheres based on the interactions between nano-size particles, which are organized in a fibrous and porous hydrogel. The process is due to a phenomenon of coacervation consisting in a solution of macromolecules which undergoes liquid-liquid phase separation leading to a polymer-rich dense phase, followed by organized merging and coalescence. The hydrogel formation process is actually similar to the behavior of tropoelastin, which is the monomer for *in vivo* elastin formation.[68] In the case of tropoelastin, chemical cross-linking of lysine motifs is needed to stabilize the hydrogel. We assumed that in our case, the presence of the PTMC domains helped to stabilize the system, acting as physical cross-links. However, as described above, syneresis occurs when we increased the concentration to 5 % w/v, probably due to a high amount of water which destabilize the coacervates formed through unstable internal pressure. This study has shown the potential of hybrid-ELPs to form relatively soft free-standing hydrogels at concentrations as low as 4 % w/v, which can be used for biomedical applications as an injectable biomaterial or a soft scaffold for tissue engineering. In addition, at low concentration, this triblock ABC could be appealing through its ability to form micelles at low temperature, which undergoes monodisperse coacervates upon heating, a feature that could be of interest for delivery systems.

ASSOCIATED CONTENT

Supporting Information. The Supporting Information is available free of charge on the ACS Publications website at DOI:

Additional experimental data including NMR, DSC, SDS-PAGE, MALDI, SEC, Turbidity, DLS, AFM, TEM) (PDF)

AUTHOR INFORMATION

Corresponding Author

*E-mail: sebastien.lecommandoux@u-bordeaux.fr

Notes

The authors declare no competing financial interest.

ACKNOWLEDGMENT

REFERENCES

(1)   Kopeček, J. Swell Gels. *Nature* **2002**, *417* (6887), 389–391. https://doi.org/10.1038/417388a.

(2)   Seiffert, S.; Sprakel, J. Physical Chemistry of Supramolecular Polymer Networks. *Chem. Soc. Rev.* **2012**, *41* (2), 909–930. https://doi.org/10.1039/C1CS15191F.

(3)   Varaprasad, K.; Raghavendra, G. M.; Jayaramudu, T.; Yallapu, M. M.; Sadiku, R. A Mini Review on Hydrogels Classification and Recent Developments in Miscellaneous Applications. *Mater. Sci. Eng. C* **2017**, *79*, 958–971. https://doi.org/https://doi.org/10.1016/j.msec.2017.05.096.

(4)   Knipe, J. M.; Peppas, N. A. Multi-Responsive Hydrogels for Drug Delivery and Tissue Engineering Applications. *Regen. Biomater.* **2014**, *1* (1), 57–65. https://doi.org/10.1093/rb/rbu006.

(5)   Sood, N.; Bhardwaj, A.; Mehta, S.; Mehta, A. Stimuli-Responsive Hydrogels in Drug Delivery and Tissue Engineering. *Drug Deliv.* **2016**, *23* (3), 748–770. https://doi.org/10.3109/10717544.2014.940091.

(6)   Hocine, S.; Li, M.-H. Thermoresponsive Self-Assembled Polymer Colloids in Water. *Soft Matter* **2013**, *9* (25), 5839–5861. https://doi.org/10.1039/C3SM50428J.

(7)   Kim, Y.-J.; Matsunaga, Y. T. Thermo-Responsive Polymers and Their Application as Smart Biomaterials. *J. Mater. Chem. B* **2017**, *5* (23), 4307–4321. https://doi.org/10.1039/C7TB00157F.

(8)   Roy, D.; Brooks, W. L. A.; Sumerlin, B. S. New Directions in Thermoresponsive Polymers. *Chem. Soc. Rev.* **2013**, *42* (17), 7214–7243. https://doi.org/10.1039/C3CS35499G.

(9)   Seuring, J.; Agarwal, S. Polymers with Upper Critical Solution Temperature in Aqueous Solution: Unexpected Properties from Known Building Blocks. *ACS Macro Lett.* **2013**, *2* (7), 597–600. https://doi.org/10.1021/mz400227y.

(10)   Tenhu, H.; Niskanen, J. How to Manipulate the Upper Critical Solution Temperature (UCST)? *Polym. Chem.* **2016**, *8*. https://doi.org/10.1039/C6PY01612J.

(11)   Hoffman, A. S. Hydrogels for Biomedical Applications. *Adv. Drug Deliv. Rev.* **2012**, *64*, 18–23. https://doi.org/https://doi.org/10.1016/j.addr.2012.09.010.

(12)   Slaughter, B. V; Khurshid, S. S.; Fisher, O. Z.; Khademhosseini, A.; Peppas, N. A. Hydrogels in Regenerative Medicine. *Adv. Mater.* **2009**, *21* (32–33), 3307–3329. https://doi.org/10.1002/adma.200802106.

(13)   Brown, T. E.; Anseth, K. S. Spatiotemporal Hydrogel Biomaterials for Regenerative Medicine. *Chem. Soc. Rev.* **2017**, *46* (21), 6532–6552. https://doi.org/10.1039/c7cs00445a.

(14)   Ghobril, C.; Grinstaff, M. W. The Chemistry and Engineering of Polymeric Hydrogel Adhesives for Wound Closure: A Tutorial. *Chem. Soc. Rev.* **2015**, *44* (7), 1820–1835. https://doi.org/10.1039/C4CS00332B.

(15)   Yang, J.-A.; Yeom, J.; Hwang, B. W.; Hoffman, A. S.; Hahn, S. K. In Situ-Forming Injectable Hydrogels for Regenerative Medicine. *Prog. Polym. Sci.* **2014**, *39* (12), 1973–1986. https://doi.org/https://doi.org/10.1016/j.progpolymsci.2014.07.006.

(16)   Geckil, H.; Xu, F.; Zhang, X.; Moon, S.; Demirci, U. Engineering Hydrogels as Extracellular Matrix Mimics. *Nanomedicine (Lond).* **2010**, *5* (3), 469–484. https://doi.org/10.2217/nnm.10.12.

(17)   Jeong, K.-H.; Park, D.; Lee, Y.-C. Polymer-Based Hydrogel Scaffolds for Skin Tissue Engineering Applications: A Mini-Review. *J. Polym. Res.* **2017**, *24* (7), 112. https://doi.org/10.1007/s10965-017-1278-4.

(18)   Ma, Y.; Tang, Y.; Billingham, N. C.; Armes, S. P.; Lewis, A. L. Synthesis of Biocompatible, Stimuli-Responsive, Physical Gels Based on ABA Triblock Copolymers. *Biomacromolecules* **2003**, *4* (4), 864–868. https://doi.org/10.1021/bm034118u.

(19)   Li, C.; Tang, Y.; Armes, S. P.; Morris, C. J.; Rose, S. F.; Lloyd, A. W.; Lewis, A. L. Synthesis and Characterization of Biocompatible Thermo-Responsive Gelators Based on ABA Triblock Copolymers. *Biomacromolecules* **2005**, *6* (2), 994–999. https://doi.org/10.1021/bm049331k.

(20)   Gohy, J.-F. Block Copolymer Micelles. In *Advances in Polymer Science*; 2005; Vol. 190, pp 65–136. https://doi.org/10.1007/12_048.

(21)   Hamley, I. W. *The Physics of Block Copolymers*; Oxford Univ. Press: Oxford, 2003.

(22)   Li, C.; Buurma, N. J.; Haq, I.; Turner, C.; Armes, S. P.; Castelletto, V.; Hamley, I. W.; Lewis, A. L. Synthesis and Characterization of Biocompatible, Thermoresponsive ABC and ABA Triblock Copolymer Gelators. *Langmuir* **2005**, *21* (24), 11026–11033. https://doi.org/10.1021/la0515672.

(23)   Taribagil, R. R.; Hillmyer, M. A.; Lodge, T. P. Hydrogels from ABA and ABC Triblock Polymers. *Macromolecules* **2010**, *43* (12), 5396–5404. https://doi.org/10.1021/ma100464z.

(24)   Taribagil, R. R.; Hillmyer, M. A.; Lodge, T. P. A Compartmentalized Hydrogel from a Linear ABC Terpolymer. *Macromolecules* **2009**, *42* (6), 1796–1800. https://doi.org/10.1021/ma8025089.

(25)   Schild, H. G. Poly(N-Isopropylacrylamide): Experiment, Theory and Application. *Prog. Polym. Sci.* **1992**, *17* (2), 163–249. https://doi.org/https://doi.org/10.1016/0079-6700(92)90023-R.

(26)   Halperin, A.; Kröger, M.; Winnik, F. M. Poly(N-isopropylacrylamide) Phase Diagrams: Fifty Years of Research. *Angew. Chemie Int. Ed.* **2015**, *54* (51), 15342–15367. https://doi.org/10.1002/anie.201506663.

(27)   Constantinou, A. P.; Georgiou, T. K. Thermoresponsive Gels Based on ABC Triblock Copolymers: Effect of the Length of the PEG Side Group. *Polym. Chem.* **2016**, *7* (11), 2045–2056. https://doi.org/10.1039/C5PY02072G.

(28)   Hu, B.; Fu, W.; Zhao, B. Enhancing Gelation of Doubly Thermosensitive Hydrophilic ABC Linear Triblock Copolymers in Water by Thermoresponsive Hairy Nanoparticles. *Macromolecules* **2016**, *49* (15), 5502–5513. https://doi.org/10.1021/acs.macromol.6b01156.

(29)   Zhou, C.; Hillmyer, M. A.; Lodge, T. P. Micellization and Micellar Aggregation of Poly(Ethylene-Alt-Propylene)-b-Poly(Ethylene Oxide)-b-Poly(N-Isopropylacrylamide) Triblock Terpolymers in Water. *Macromolecules* **2011**, *44* (6), 1635–1641. https://doi.org/10.1021/ma102786q.

(30)   Zhou, C.; Hillmyer, M. A.; Lodge, T. P. Efficient Formation of Multicompartment Hydrogels by Stepwise Self-Assembly of Thermoresponsive ABC Triblock Terpolymers. *J. Am. Chem. Soc.* **2012**, *134* (25), 10365–10368. https://doi.org/10.1021/ja303841f.

(31)   Zhou, C.; Toombes, G. E. S.; Wasbrough, M. J.; Hillmyer, M. A.; Lodge, T. P. Structure of Two-Compartment Hydrogels from Thermoresponsive ABC Triblock Terpolymers. *Macromolecules* **2015**, *48* (16), 5934–5943. https://doi.org/10.1021/acs.macromol.5b00584.

(32)   Hall, C. C.; Zhou, C.; Danielsen, S. P. O.; Lodge, T. P. Formation of Multicompartment Ion Gels by Stepwise Self-Assembly of a Thermoresponsive ABC Triblock Terpolymer in an Ionic Liquid. *Macromolecules* **2016**, *49* (6), 2298–2306. https://doi.org/10.1021/acs.macromol.5b02789.

(33)   Koonar, I.; Zhou, C.; Hillmyer, M. A.; Lodge, T. P.; Siegel, R. A. ABC Triblock Terpolymers Exhibiting Both Temperature- and PH-Sensitive Micellar Aggregation and Gelation in Aqueous Solution. *Langmuir* **2012**, *28* (51), 17785–17794. https://doi.org/10.1021/la303712b.

(34)   Gupta, M. K.; Martin, J. R.; Werfel, T. A.; Shen, T.; Page, J. M.; Duvall, C. L. Cell Protective, ABC Triblock Polymer-Based Thermoresponsive Hydrogels with ROS-Triggered Degradation and Drug Release. *J. Am. Chem. Soc.* **2014**, *136* (42), 14896–14902. https://doi.org/10.1021/ja507626y.

(35)   Dollinger, B. R.; Gupta, M. K.; Martin, J. R.; Duvall, C. L. Reactive Oxygen Species Shielding Hydrogel for the Delivery of Adherent and Nonadherent Therapeutic Cell Types. *Tissue Eng. Part A* **2017**, *23* (19–20), 1120–1131. https://doi.org/10.1089/ten.tea.2016.0495.

(36)   Gupta, M. K.; Martin, J. R.; Dollinger, B. R.; Hattaway, M. E.; Duvall, C. L. Thermogelling, ABC Triblock Copolymer Platform for Resorbable Hydrogels with Tunable, Degradation-Mediated Drug Release. *Adv. Funct. Mater.* **2017**, *27* (47), 1704107. https://doi.org/10.1002/adfm.201704107.

(37)   Fukushima, K. Poly(Trimethylene Carbonate)-Based Polymers Engineered for Biodegradable Functional Biomaterials. *Biomater. Sci.* **2016**, *4* (1), 9–24. https://doi.org/10.1039/C5BM00123D.

(38)   Roberts, S.; Dzuricky, M.; Chilkoti, A. Elastin-like Polypeptides as Models of Intrinsically Disordered Proteins. *FEBS Lett.* **2015**, *589* (19, Part A), 2477–2486. https://doi.org/https://doi.org/10.1016/j.febslet.2015.08.029.

(39) Meyer, D. E.; Chilkoti, A. Purification of Recombinant Proteins by Fusion with Thermally-Responsive Polypeptides. *Nat. Biotechnol.* **1999**, *17* (11), 1112–1115. https://doi.org/10.1038/15100.

(40) Meyer, D. E.; Chilkoti, A. Quantification of the Effects of Chain Length and Concentration on the Thermal Behavior of Elastin-like Polypeptides. *Biomacromolecules* **2004**, *5* (3), 846–851. https://doi.org/10.1021/bm034215n.

(41) Cho, Y.; Zhang, Y.; Christensen, T.; Sagle, L. B.; Chilkoti, A.; Cremer, P. S. Effects of Hofmeister Anions on the Phase Transition Temperature of Elastin-like Polypeptides. *J. Phys. Chem. B* **2008**, *112* (44), 13765–13771. https://doi.org/10.1021/jp8062977.

(42) Urry, D. W.; Gowda, D. C.; Parker, T. M.; Luan, C.-H.; Reid, M. C.; Harris, C. M.; Pattanaik, A.; Harris, R. D. Hydrophobicity Scale for Proteins Based on Inverse Temperature Transitions. *Biopolymers* **1992**, *32* (9), 1243–1250. https://doi.org/10.1002/bip.360320913.

(43) Yeo, G. C.; Aghaei-Ghareh-Bolagh, B.; Brackenreg, E. P.; Hiob, M. A.; Lee, P.; Weiss, A. S. Fabricated Elastin. *Adv. Healthc. Mater.* **2015**, *4* (16), 2530–2556. https://doi.org/10.1002/adhm.201400781.

(44) Ramamurthi, A.; Kothapalli, C. *Elastic Fiber Matrices Biomimetic Approaches to Regeneration and Repair*; CRC Press, 2016.

(45) Coenen, A. M. J.; Bernaerts, K. V; Harings, J. A. W.; Jockenhoevel, S.; Ghazanfari, S. Elastic Materials for Tissue Engineering Applications: Natural, Synthetic, and Hybrid Polymers. *Acta Biomater.* **2018**, *79*, 60–82. https://doi.org/https://doi.org/10.1016/j.actbio.2018.08.027.

(46) Mithieux, S. M.; Wise, S. G.; Weiss, A. S. Tropoelastin — A Multifaceted Naturally Smart Material. *Adv. Drug Deliv. Rev.* **2013**, *65* (4), 421–428. https://doi.org/https://doi.org/10.1016/j.addr.2012.06.009.

(47) Wise, S. G.; Yeo, G. C.; Hiob, M. A.; Rnjak-Kovacina, J.; Kaplan, D. L.; Ng, M. K. C.; Weiss, A. S. Tropoelastin: A Versatile, Bioactive Assembly Module. *Acta Biomater.* **2014**, *10* (4), 1532–1541. https://doi.org/10.1016/j.actbio.2013.08.003.

(48) Wang, H.; Cai, L.; Paul, A.; Enejder, A.; Heilshorn, S. C. Hybrid Elastin-like Polypeptide–Polyethylene Glycol (ELP-PEG) Hydrogels with Improved Transparency and Independent Control of Matrix Mechanics and Cell Ligand Density. *Biomacromolecules* **2014**, *15* (9), 3421–3428. https://doi.org/10.1021/bm500969d.

(49) Araújo, A.; Olsen, B. D.; Machado, A. V. Engineering Elastin-Like Polypeptide-Poly(Ethylene Glycol) Multiblock Physical Networks. *Biomacromolecules* **2018**, *19* (2), 329–339. https://doi.org/10.1021/acs.biomac.7b01424.

(50) Meco, E.; Lampe, K. J. Impact of Elastin-like Protein Temperature Transition on PEG-ELP Hybrid Hydrogel Properties. *Biomacromolecules* **2019**, *20* (5), 1914–1925. https://doi.org/10.1021/acs.biomac.9b00113.

(51) Meyer, D. E.; Trabbic-Carlson, K.; Chilkoti, A. Protein Purification by Fusion with an Environmentally Responsive Elastin-Like Polypeptide: Effect of Polypeptide Length on the Purification of Thioredoxin. *Biotechnol. Prog.* **2001**, *17* (4), 720–728. https://doi.org/10.1021/bp010049o.

(52)   Meyer, D. E.; Chilkoti, A. Genetically Encoded Synthesis of Protein-Based Polymers with Precisely Specified Molecular Weight and Sequence by Recursive Directional Ligation: Examples from the Elastin-like Polypeptide System. *Biomacromolecules* **2002**, *3* (2), 357–367. https://doi.org/10.1021/bm015630n.

(53)   Bataille, L.; Dieryck, W.; Hocquellet, A.; Cabanne, C.; Bathany, K.; Lecommandoux, S.; Garbay, B.; Garanger, E. Recombinant Production and Purification of Short Hydrophobic Elastin-like Polypeptides with Low Transition Temperatures. *Protein Expr. Purif.* **2016**, *121*, 81–87. https://doi.org/https://doi.org/10.1016/j.pep.2016.01.010.

(54)   Chan, J. M. W.; Zhang, X.; Brennan, M. K.; Sardon, H.; Engler, A. C.; Fox, C. H.; Frank, C. W.; Waymouth, R. M.; Hedrick, J. L. Organocatalytic Ring-Opening Polymerization of Trimethylene Carbonate To Yield a Biodegradable Polycarbonate. *J. Chem. Educ.* **2015**, *92* (4), 708–713. https://doi.org/10.1021/ed500595k.

(55)   Pratt, R. C.; Lohmeijer, B. G. G.; Long, D. A.; Lundberg, P. N. P.; Dove, A. P.; Li, H.; Wade, C. G.; Waymouth, R. M.; Hedrick, J. L. Exploration, Optimization, and Application of Supramolecular Thiourea−Amine Catalysts for the Synthesis of Lactide (Co)Polymers. *Macromolecules* **2006**, *39* (23), 7863–7871. https://doi.org/10.1021/ma061607o.

(56)   Tripathi, C. B.; Mukherjee, S. Lewis Base Catalysis by Thiourea: N-Bromosuccinimide-Mediated Oxidation of Alcohols. *J. Org. Chem.* **2012**, *77* (3), 1592–1598. https://doi.org/10.1021/jo202269p.

(57)   Sun, J.; Kuckling, D. *Synthesis of High-Molecular-Weight Aliphatic Polycarbonates by Organo-Catalysis*; 2016; Vol. 7. https://doi.org/10.1039/C5PY01843A.

(58)   Xiao, Y.; Chinoy, Z. S.; Pecastaings, G.; Bathany, K.; Garanger, E.; Lecommandoux, S. Design of Polysaccharide-b-Elastin-Like Polypeptide Bioconjugates and Their Thermoresponsive Self-Assembly. *Biomacromolecules* **2020**, *21* (1), 114–125. https://doi.org/10.1021/acs.biomac.9b01058.

(59)   Zhu, K. J.; Hendren, R. W.; Jensen, K.; Pitt, C. G. Synthesis, Properties, and Biodegradation of Poly(1,3-Trimethylene Carbonate). *Macromolecules* **1991**, *24* (8), 1736–1740. https://doi.org/10.1021/ma00008a008.

(60)   Kramer, J. R.; Petitdemange, R.; Bataille, L.; Bathany, K.; Wirotius, A.-L.; Garbay, B.; Deming, T. J.; Garanger, E.; Lecommandoux, S. Quantitative Side-Chain Modifications of Methionine-Containing Elastin-Like Polypeptides as a Versatile Tool to Tune Their Properties. *ACS Macro Lett.* **2015**, *4* (11), 1283–1286. https://doi.org/10.1021/acsmacrolett.5b00651.

(61)   Petitdemange, R.; Garanger, E.; Bataille, L.; Bathany, K.; Garbay, B.; Deming, T. J.; Lecommandoux, S. Tuning Thermoresponsive Properties of Cationic Elastin-like Polypeptides by Varying Counterions and Side-Chains. *Bioconjug. Chem.* **2017**, *28* (5), 1403–1412. https://doi.org/10.1021/acs.bioconjchem.7b00082.

(62)   Petitdemange, R.; Garanger, E.; Bataille, L.; Dieryck, W.; Bathany, K.; Garbay, B.; Deming, T. J.; Lecommandoux, S. Selective Tuning of Elastin-like Polypeptide Properties via Methionine Oxidation. *Biomacromolecules* **2017**, *18* (2), 544–550. https://doi.org/10.1021/acs.biomac.6b01696.

(63)   Alemán, E. A.; Pedini, H. S.; Rueda, D. Covalent-Bond-Based Immobilization Approaches for Single-Molecule Fluorescence. *Chembiochem* **2009**, *10* (18), 2862–2866. https://doi.org/10.1002/cbic.200900640.

(64) Janib, S. M.; Pastuszka, M.; Aluri, S.; Folchman-Wagner, Z.; Hsueh, P.-Y.; Shi, P.; Yi-An; Cui, H.; Mackay, J. A. A Quantitative Recipe for Engineering Protein Polymer Nanoparticles. *Polym. Chem.* **2014**, *5* (5), 1614–1625. https://doi.org/10.1039/C3PY00537B.

(65) Gan, T.; Guan, Y.; Zhang, Y. Thermogelable PNIPAM Microgel Dispersion as 3D Cell Scaffold: Effect of Syneresis. *J. Mater. Chem.* **2010**, *20*, 5937–5944. https://doi.org/10.1039/c0jm00338g.

(66) Bischofberger, I.; Trappe, V. New Aspects in the Phase Behaviour of Poly-N-Isopropyl Acrylamide: Systematic Temperature Dependent Shrinking of PNiPAM Assemblies Well beyond the LCST. *Sci. Rep.* **2015**, *5* (1), 15520. https://doi.org/10.1038/srep15520.

(67) Elbert, D. L. Liquid-Liquid Two-Phase Systems for the Production of Porous Hydrogels and Hydrogel Microspheres for Biomedical Applications: A Tutorial Review. *Acta Biomater.* **2011**, *7* (1), 31–56. https://doi.org/10.1016/j.actbio.2010.07.028.

(68) Tu, Y.; Wise, S. G.; Weiss, A. S. Stages in Tropoelastin Coalescence during Synthetic Elastin Hydrogel Formation. *Micron* **2010**, *41* (3), 268–272. https://doi.org/https://doi.org/10.1016/j.micron.2009.11.003.

Supporting Information for:

Thermosensitive hybrid elastin-like polypeptide-based ABC triblock hydrogel

Michèle Dai,[†,‡] Guillaume Goudounet,[†] Hang Zhao,[†] Bertrand Garbay,[†] Elisabeth Garanger,[†] Gilles Pecastaings,[†] Xavier Schultze,[‡] and Sébastien Lecommandoux[,†]*

[†] Univ. Bordeaux, CNRS, Bordeaux INP, LCPO, UMR 5629, F-33600, Pessac, France

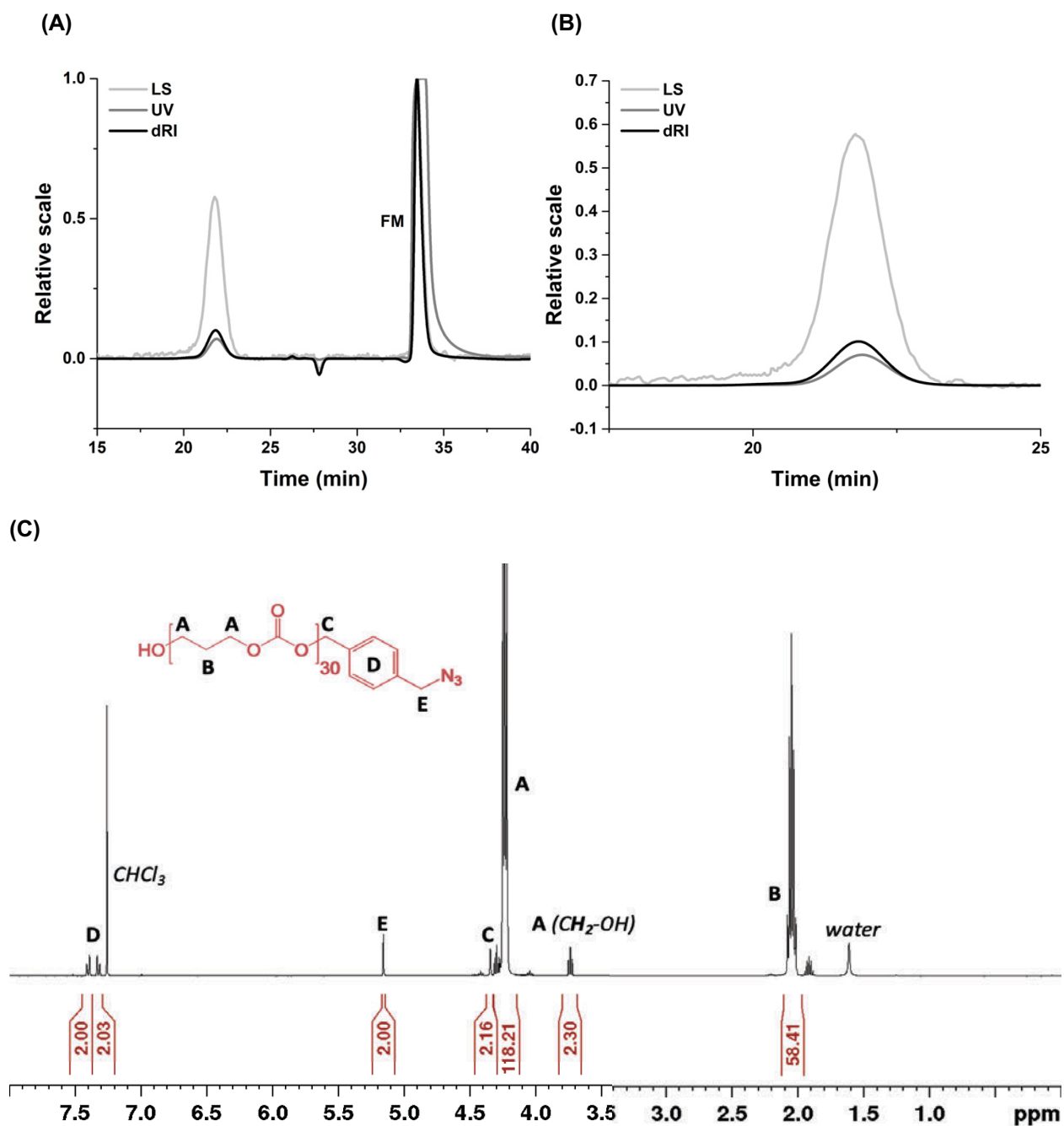[‡] L'Oréal Recherche Avancée, 1 avenue Eugène Schueller, 93600, Aulnay-sous-Bois, France

Figure S1. **(A)** Triple detection size exclusion chromatography of PTMC$_{30}$-N$_3$ analysis in *N,N*-dimethylformamide (DMF) + 1 g/L LiBr with : - Light scattering (LS) detection; - Ultraviolet (UV) detection ; **-** Differential refractive index (dRI) detection. Đ = 1.01 determined from dRI *spectrum*. FM = Flow marker: Toluene. **(B)** Zoom on PTMC$_{30}$-N$_3$ peak. **(C)** ^{1}H NMR *spectrum* of PTMC$_{30}$-N$_3$ in CDCl$_{3.}$

```
atgtgggttccaggcgttggagtgccaggcatgggcgtaccaggtgtgggagttccaggt
 M   W   V   P   G   V   G   V   P   G   M   G   V   P   G   V   G   V   P   G
gttggggtaccgggcgtcggagttcctgggatgggagttccgggagttggtgtgccgggt
 V   G   V   P   G   V   G   V   P   G   M   G   V   P   G   V   G   V   P   G
gtcggtgtgcctggggtgggtgttccaggtatgggggttccgggtgtcggcgttcccggc
 V   G   V   P   G   V   G   V   P   G   M   G   V   P   G   V   G   V   P   G
gttggtgttccaggcgtaggtgtaccgggaatgggggttccgggagttggtgtacctggc
 V   G   V   P   G   V   G   V   P   G   M   G   V   P   G   V   G   V   P   G
gtgggagtacctggagtcggcgtgcctggtatgggcgtgcctggcgtcggcgtacctggc
 V   G   V   P   G   V   G   V   P   G   M   G   V   P   G   V   G   V   P   G
gtaggtgttccaggcgttggagtgccaggcatgggcgtaccaggtgtgggagttccaggt
 V   G   V   P   G   V   G   V   P   G   M   G   V   P   G   V   G   V   P   G
gttggggtaccgggcgtcggagttcctgggatgggagttccgggagttggtgtgccgggt
 V   G   V   P   G   V   G   V   P   G   M   G   V   P   G   V   G   V   P   G
gtcggtgtgcctggggtgggtgttccaggtatgggggttccgggtgtcggcgttcccggc
 V   G   V   P   G   V   G   V   P   G   M   G   V   P   G   V   G   V   P   G
gttggtgttccaggcgtaggtgtgccgggaatgggggttccgggagttggtgtacctggc
 V   G   V   P   G   V   G   V   P   G   M   G   V   P   G   V   G   V   P   G
gtgggagtacctggagtcggcgtgcctggtatgggcgtgcctggcgtcggcgtacctggc
 V   G   V   P   G   V   G   V   P   G   M   G   V   P   G   V   G   V   P   G
gtaggtgttccaggcgttggagtgccaggcatgggcgtaccaggtgtgggagttccaggt
 V   G   V   P   G   V   G   V   P   G   M   G   V   P   G   V   G   V   P   G
gttggggtaccgggcgtcggagttcctgggatgggagttccgggagttggtgtgccgggt
 V   G   V   P   G   V   G   V   P   G   M   G   V   P   G   V   G   V   P   G
gtcggtgtgcctggggtgggtgttccaggtatgggggttccgggtgtcggcgttcccggc
 V   G   V   P   G   V   G   V   P   G   M   G   V   P   G   V   G   V   P   G
gttggtgttccaggcgtaggtgtgccgggaatgggggttccgggagttggtgtacctggc
 V   G   V   P   G   V   G   V   P   G   M   G   V   P   G   V   G   V   P   G
gtgggagtacctggagtcggcgtgcctggtatgggcgtgcctggcgtcggcgtacctggc
 V   G   V   P   G   V   G   V   P   G   M   G   V   P   G   V   G   V   P   G
gtaggtgttccaggcattggagtgccaggcattggcgtaccaggtattggagttccaggt
 V   G   V   P   G   I   G   V   P   G   I   G   V   P   G   I   G   V   P   G
attggggtaccgggcatcggagttcctgggatcggagttccgggaattggtgtgccgggt
 I   G   V   P   G   I   G   V   P   G   I   G   V   P   G   I   G   V   P   G
atcggtgtgcctgggatcggtgttccaggtatcggggttccgggtatcggcgttcccggc
 I   G   V   P   G   I   G   V   P   G   I   G   V   P   G   I   G   V   P   G
attggtgttccaggcatcggtgtgccgggaattggggttccggggattggtgtacctggc
 I   G   V   P   G   I   G   V   P   G   I   G   V   P   G   I   G   V   P   G
attggggtacctggaatcggcgtgcctggtattggcgtgcctggcatcggcgttcctggc
 I   G   V   P   G   I   G   V   P   G   I   G   V   P   G   I   G   V   P   G
attggttgctaa
 I   G   C   -
```

Figure S2. Sequences of the diblock MW-(ELP[V_3M_1-60])-(ELP[I_1-20])-C ELP gene and of the corresponding protein.
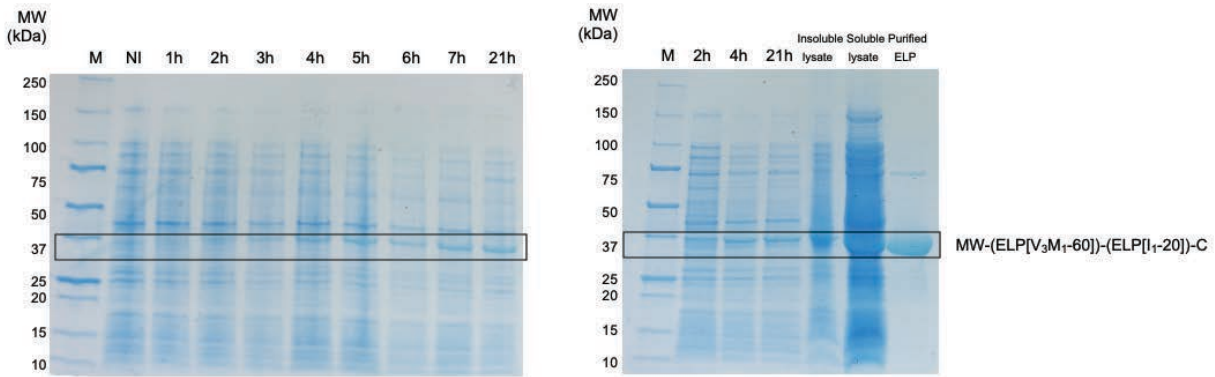
Figure S3. Expression of recombinant MW-(ELP[V_3M_1-60])-(ELP[I_1-20])-C during bacterial fermentation as analyzed by SDS-PAGE; M = molecular weight marker; NI = Non-induced culture; time in hours = culture time after induction; Insoluble and soluble lysates; Purified ELP.
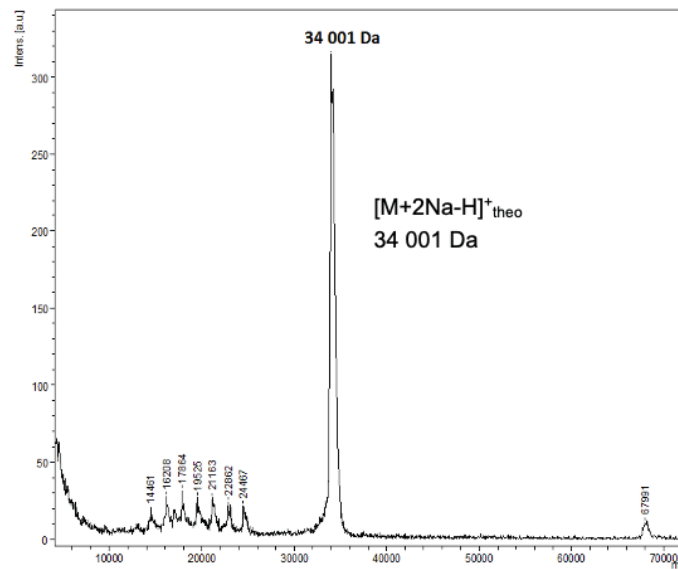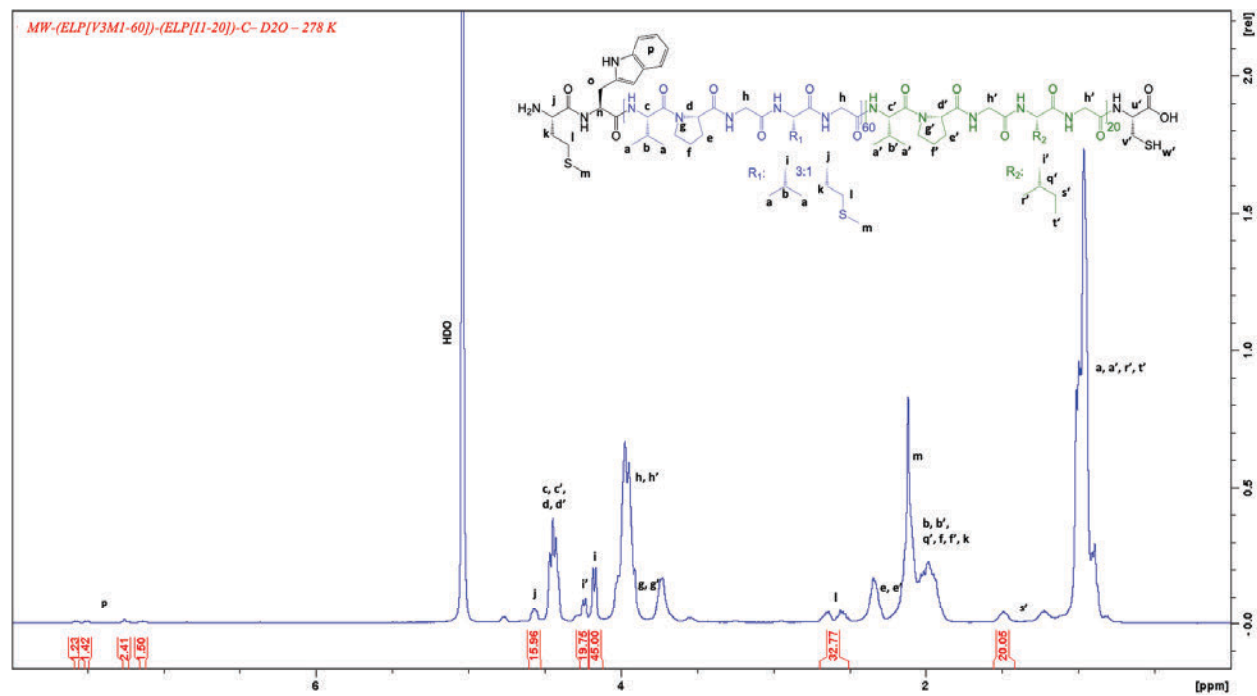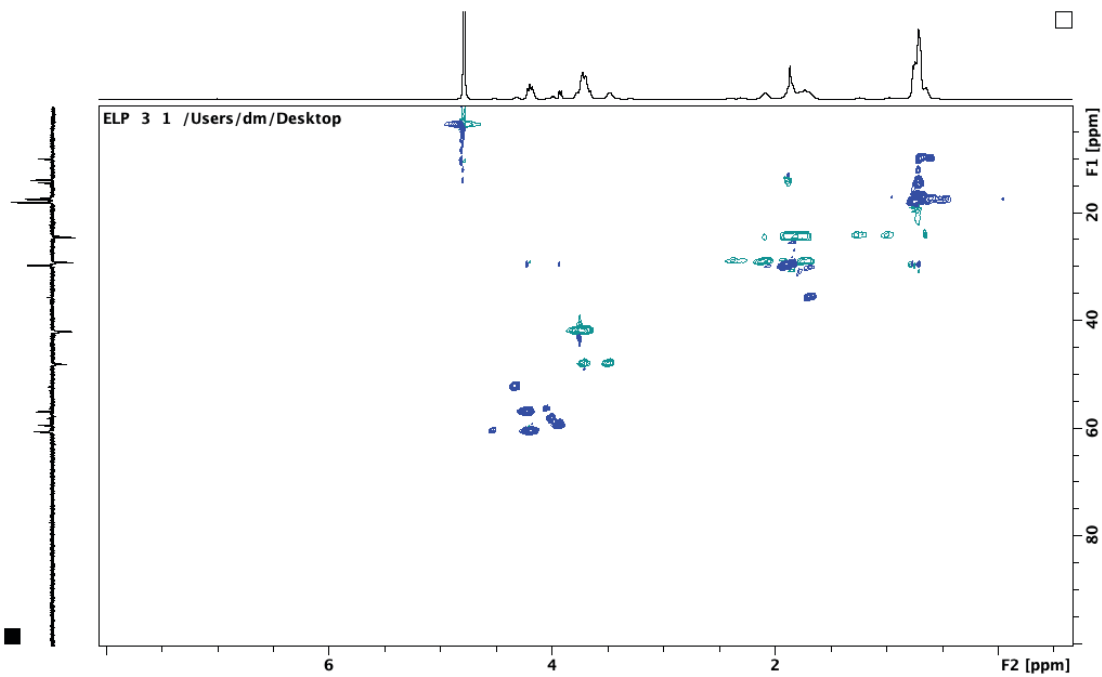

Figure S4. MALDI mass *spectrum* of MW-(ELP[V_3M_1-60])-(ELP[I_1-20])-C. [M+2Na-H]$^+_{theo}$ = theoretical mass of monocharged species.
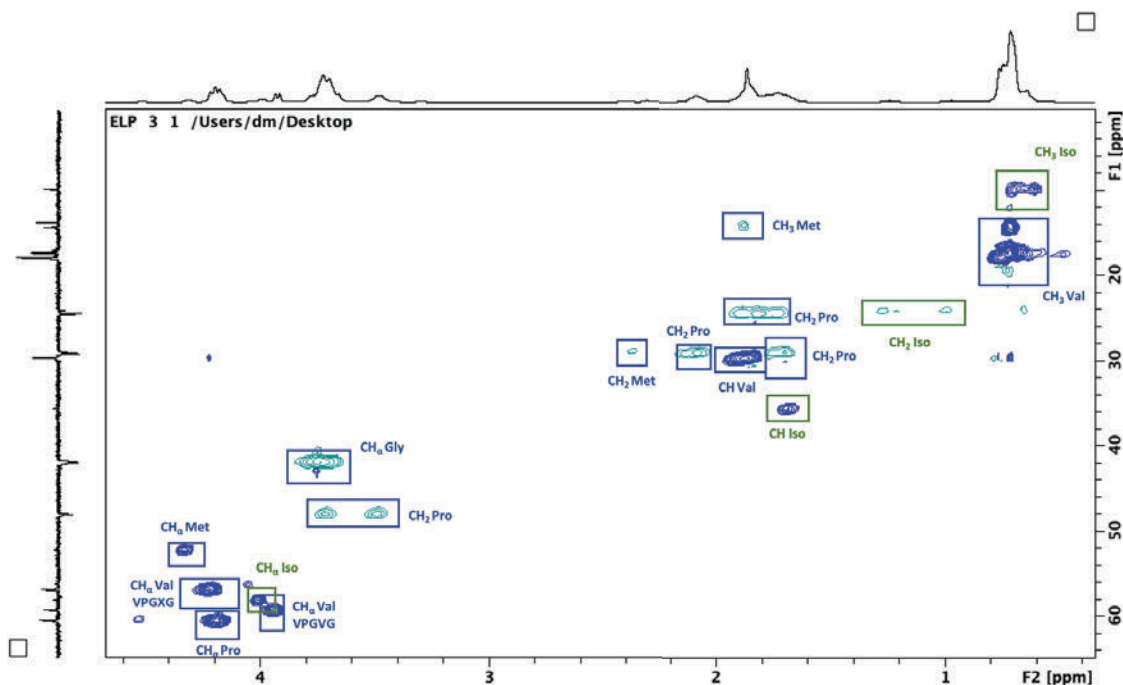
(A)

(B)

Figure S5. MW-(ELP[V_3M_1-60])-(ELP[I_1-20])-C NMR *spectra* in D_2O at 278K. (**A**) 1H (**B**) HSQC; top: full *spectrum*, down: expanded region. HSQC analyses were performed on a Bruker AVANCE NEO 400 spectrometer operating at 100.7 equipped with a 5 mm Bruker multinuclear z-gradient direct cryoprobe-head operating at 278 K. Peaks were easily assigned as *spectra* from **MW-**ELP[V_3M_1-40] and MW-ELP[I_1-20] are known.[2, 3]

[2] Bataille, L.; Dieryck, W.; Hocquellet, A.; Cabanne, C.; Bathany, K.; Lecommandoux, S.; Garbay, B.; Garanger, E. Recombinant Production and Purification of Short Hydrophobic Elastin-like Polypeptides with Low Transition Temperatures. *Protein Expr. Purif.* **2016**, *121*, 81–87. https://doi.org/https://doi.org/10.1016/j.pep.2016.01.010.

[3] Kramer, J. R.; Petitdemange, R.; Bataille, L.; Bathany, K.; Wirotius, A.-L.; Garbay, B.; Deming, T. J.; Garanger, E.; Lecommandoux, S. Quantitative Side-Chain Modifications of Methionine-Containing Elastin-Like Polypeptides as a Versatile Tool to Tune Their Properties. *ACS Macro Lett.* **2015**, *4* (11), 1283–1286. https://doi.org/10.1021/acsmacrolett.5b00651.

Figure S6. Ring opening polymerization side-reactions: (i) intra-molecular. (ii) inter-molecular transcarbonatation. *for any degree of polymerization. (Adapted from [1])
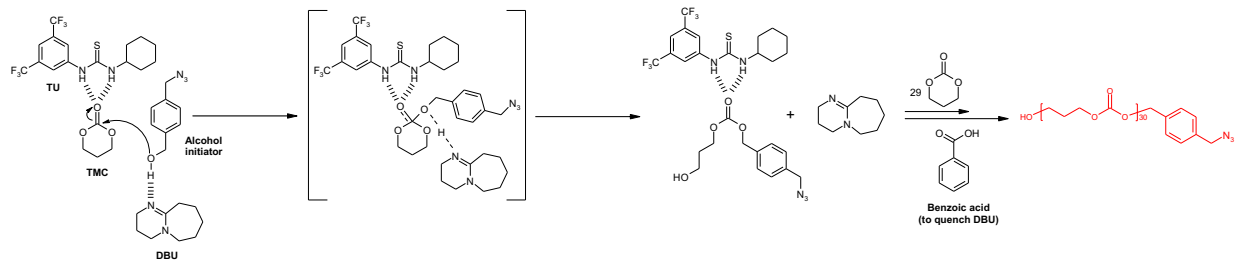
6

Figure S7. Dual-activation mechanism with thiourea-amine catalysts in a ring opening polymerization of 1,3-dioxane-2-one. (Adapted from [1])

[1] Chan, J. M. W.; Zhang, X.; Brennan, M. K.; Sardon, H.; Engler, A. C.; Fox, C. H.; Frank, C. W.; Waymouth, R. M.; Hedrick, J. L. Organocatalytic Ring-Opening Polymerization of Trimethylene Carbonate To Yield a Biodegradable Polycarbonate. *J. Chem. Educ.* **2015**, *92* (4), 708–713. https://doi.org/10.1021/ed500595k.
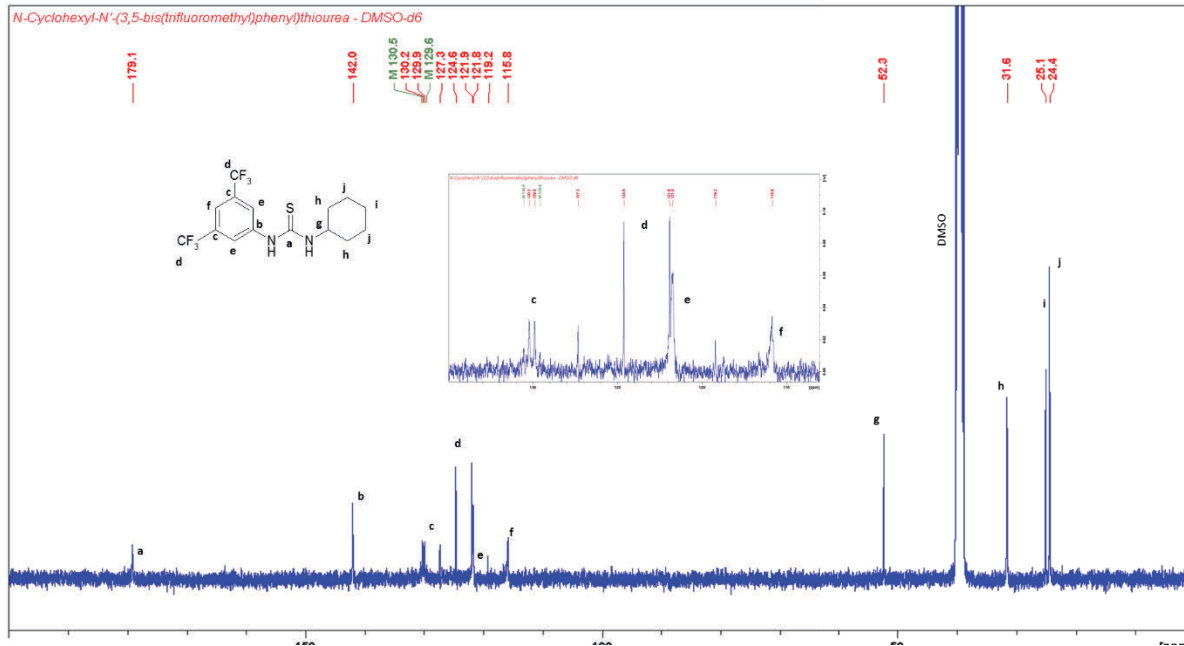
(A)
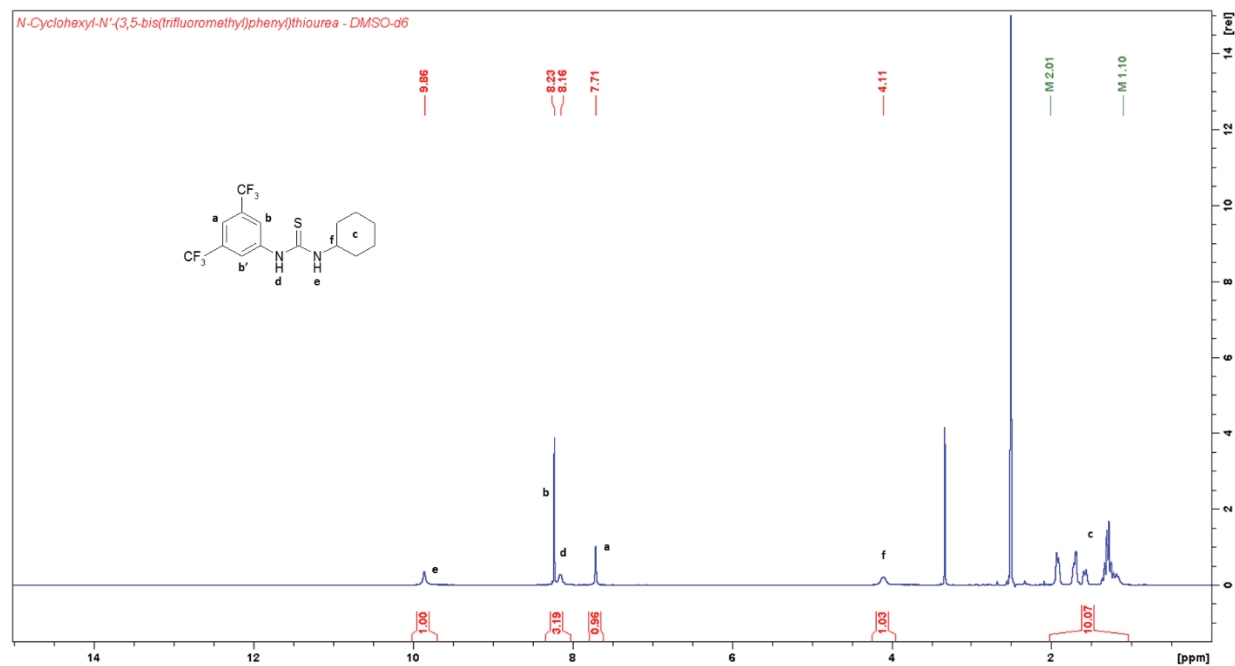
Figure S8. NMR *spectra*. **(A)** 1H and **(B)** 13C of *N*-cyclohexyl-*N'*-(3,5-bis(trifluoromethyl)phenyl) thiourea in DMSO-d6.
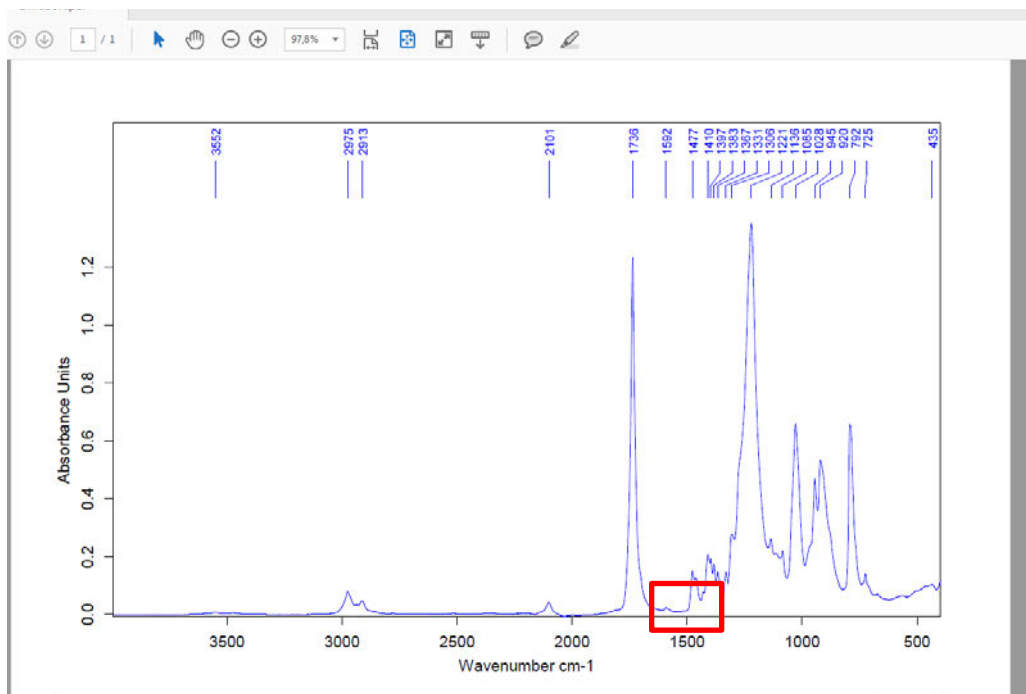
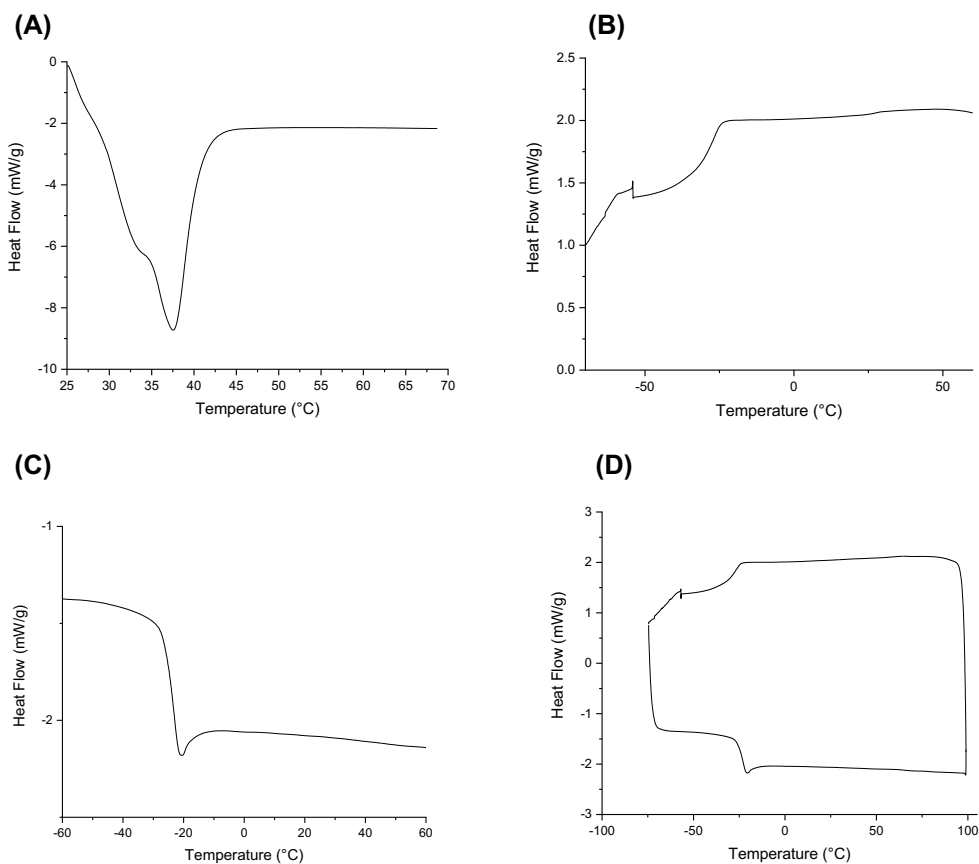**Figure S9.** Fourier-transform infrared spectroscopy (FTIR) *spectra* of PTMC$_{30}$-N$_3$.

Figure S10. Thermal analysis of PTMC$_{30}$-N$_3$ by differential scanning calorimetry (DSC) thermograms (10°C/min) **(A)** first heating **(B)** cooling **(C)** second heating **(D)** an entire cycle.
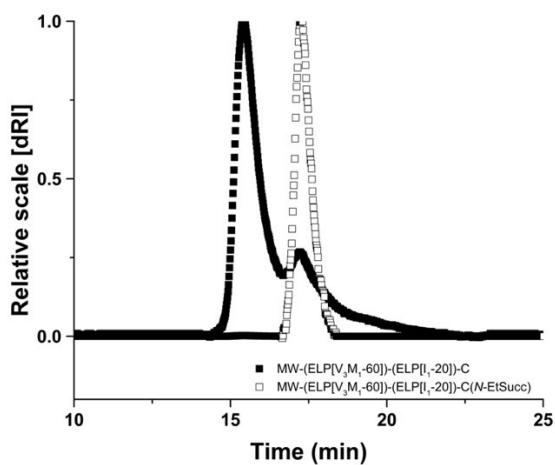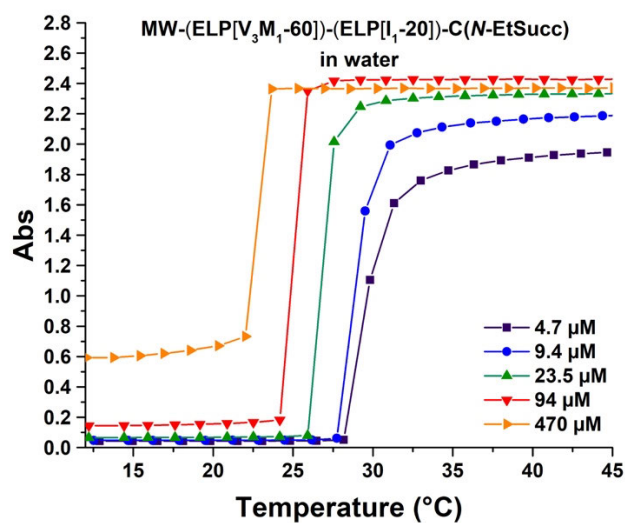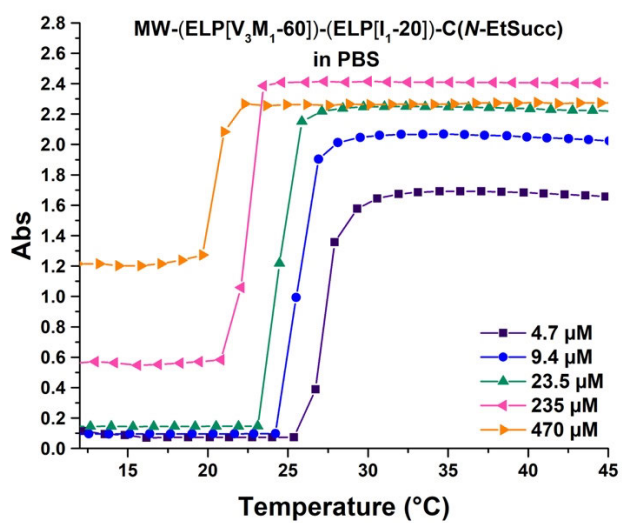

Figure S11. MW-(ELP[V$_3$M$_1$-60])-(ELP[I$_1$-20])-C and MW-(ELP[V$_3$M$_1$-60])-(ELP[I$_1$-20])-C(*N*-EtSucc) SEC dRI *spectra* in DMF.

(A) MW-(ELP[V$_3$M$_1$-60])-(ELP[I$_1$-20])-C(*N*-EtSucc) in water

- 4.7 µM
- 9.4 µM
- 23.5 µM
- 94 µM
- 470 µM

(B) MW-(ELP[V$_3$M$_1$-60])-(ELP[I$_1$-20])-C(*N*-EtSucc) in PBS

- 4.7 µM
- 9.4 µM
- 23.5 µM
- 235 µM
- 470 µM

(C) PTMC$_{30}$-*b*-MW-(ELP[V$_3$M$_1$-60])-(ELP[I$_1$-20])-C(*N*-EtSucc) in water

- 4.7 µM
- 9.4 µM
- 23.5 µM
- 47 µM
- 94 µM
- 235 µM

(D) PTMC$_{30}$-*b*-MW-(ELP[V$_3$M$_1$-60])-(ELP[I$_1$-20])-C(*N*-EtSucc) in PBS

- 4.7 µM
- 9.4 µM
- 23.5 µM
- 47 µM
- 235 µM

10

(E)

PTMC$_{30}$-*b*-MW-(ELP[V$_3$M$_1$-60])-(ELP[I$_1$-20])-C(*N*-EtSucc) in PBS
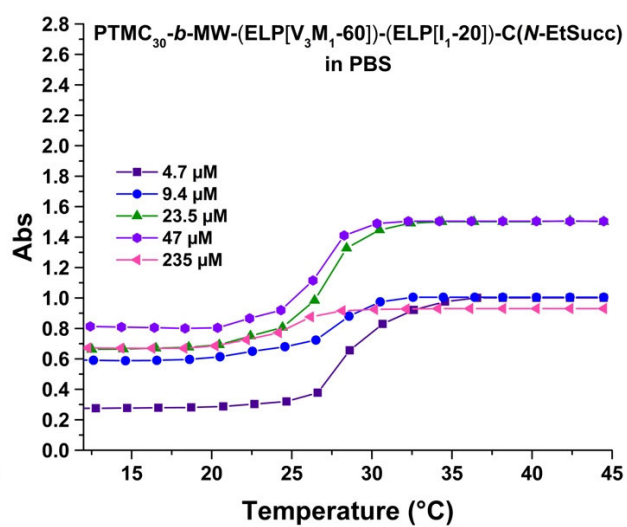
Legend:
- 4.7 µM
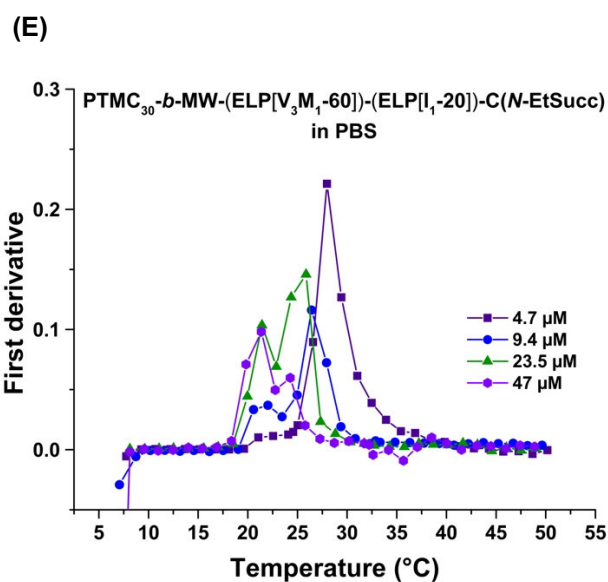- 9.4 µM
- 23.5 µM
- 47 µM
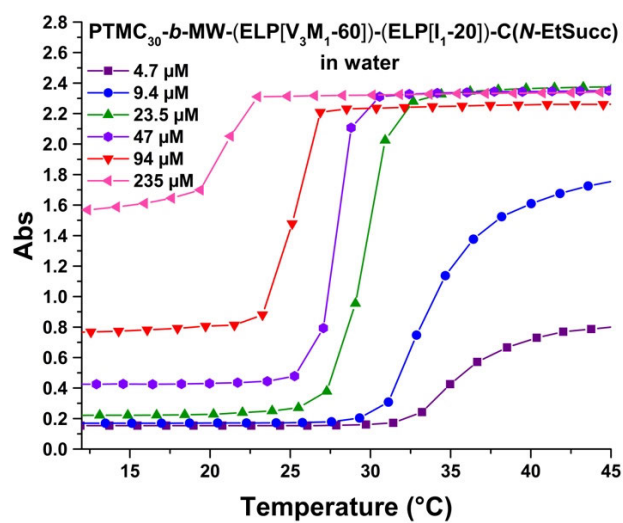
Figure S12. Turbidity assays at 350 nm with a rate of 1.5°C/min on BC diblock **(A)** in UP water and in **(B)** PBS 1X and on ABC triblock **(C)** in UP water **(D)** in PBS 1X at different concentrations. **(E)** First derivative graphs applied to (D) results to better visualize the double transition temperatures.

Data from Figure S12 have been used to estimate transition temperatures, shown in Table S1 *via* the first derivative method.

Table S1. Experimental Tt values of MW-(ELP[V$_3$M$_1$-60])-(ELP[I$_1$-20])-C(*N*-EtSucc) and PTMC$_{30}$-*b*-MW-(ELP[V$_3$M$_1$-60])-(ELP[I$_1$-20])-C(*N*-EtSucc) at different concentrations in UP water and in PBS 1X obtained by first derivative method applied on Figure S11's curves. In the table, X = no *data* acquired.

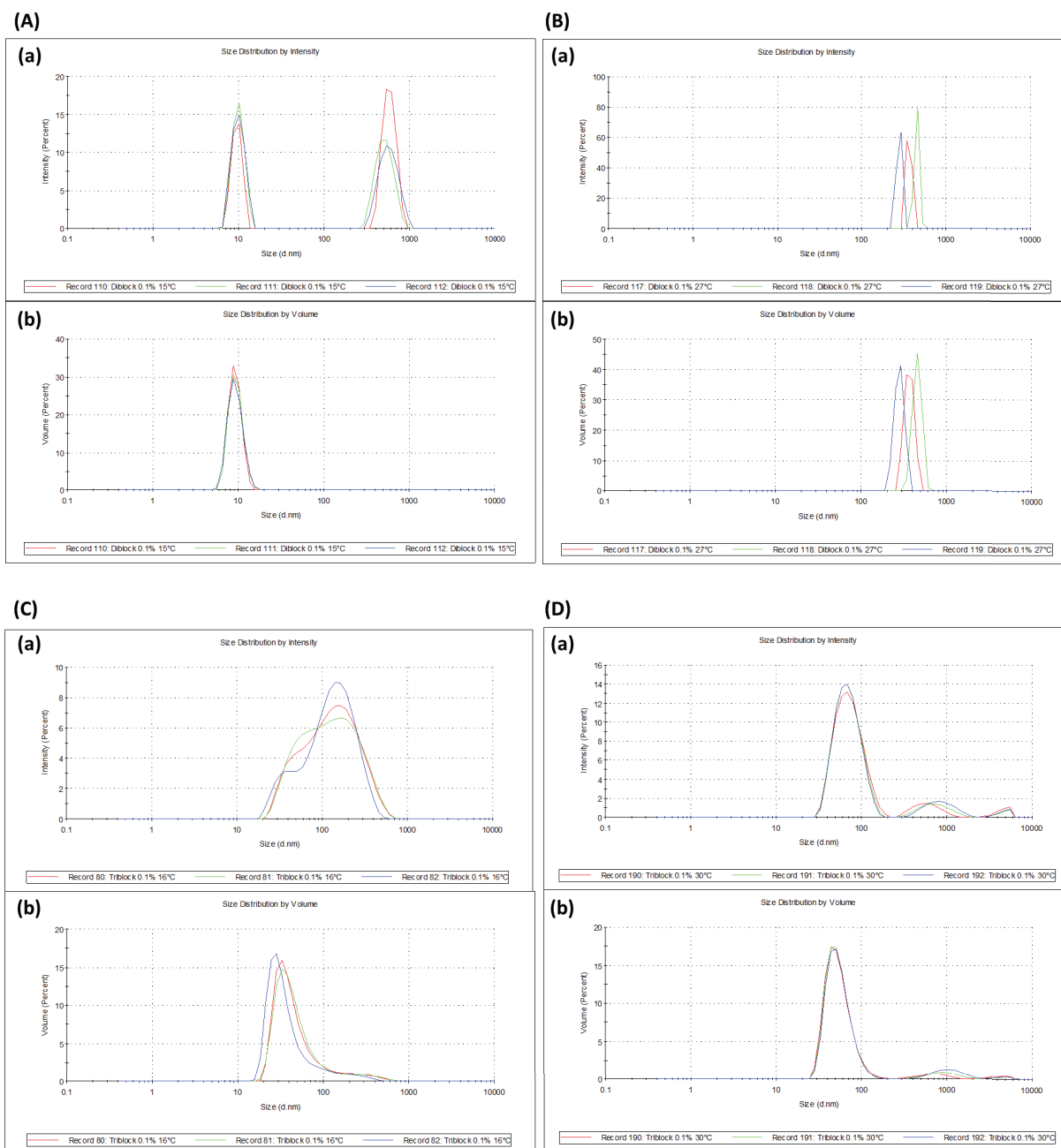| Concentration (µM)	Tt values (°C)				
	Diblock MW-(ELP[V$_3$M$_1$-60])-(ELP[I$_1$-20])-C(*N*-EtSucc)		**Triblock** PTMC$_{30}$-*b*-MW-(ELP[V$_3$M$_1$-60])-(ELP[I$_1$-20])-C(*N*-EtSucc)		
	UP water	PBS 1X	UP water	PBS 1X	
				Transition 1	Transition 2
4.7	28.2	25.8	33.2	22.0	28.0
9.4	27.8	24.5	31.1	21.9	27.9
23.5	25.9	23.1	29.1	21.8	27.0
47	X	X	27.1	21.6	27.0
94	X	X	25.1	X	X
235	23.9	19.7	21.3	20.2	24.9
470	22.0	18.9	X	X	X

11

Figure S13. Size distribution in **(a)** intensity and **(b)** volume of **(A, B)** diblock and **(C, D)** triblock at 0.1 % w/v at different temperatures **(A, C)** below their Tt and **(B, D)** above their Tt, measured *via* dynamic light scattering at a 173° scattering angle.
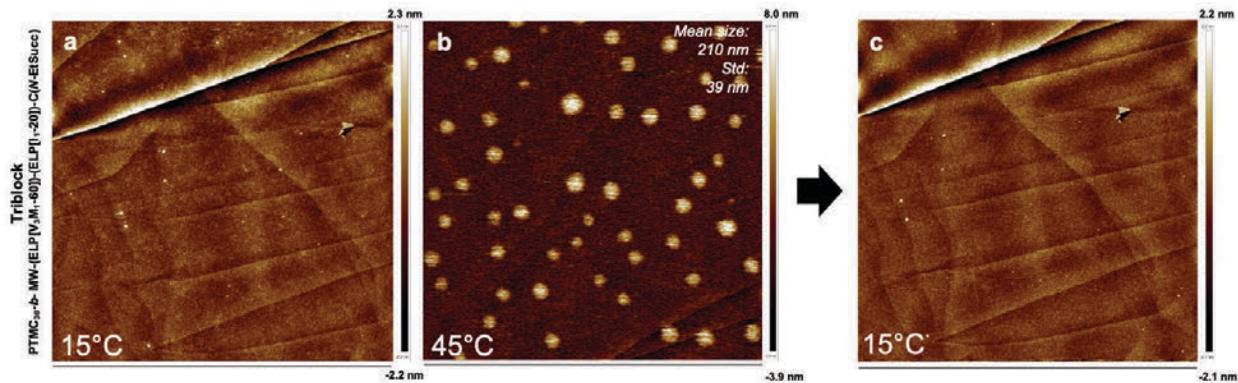
Figure S14. Liquid AFM images of PTMC$_{30}$-*b*-MW-(ELP[V$_3$M$_1$-60])-(ELP[I$_1$-20])-C(*N*-EtSucc) solution in UP water at 0.3% w/v, **(a)** cooled at T < Tt$_{triblock}$, **(b)** heated at T > Tt$_{triblock}$ and **(c)** cooled again at T < Tt$_{triblock}$, showing its reversibility. Images size: 5 µm.
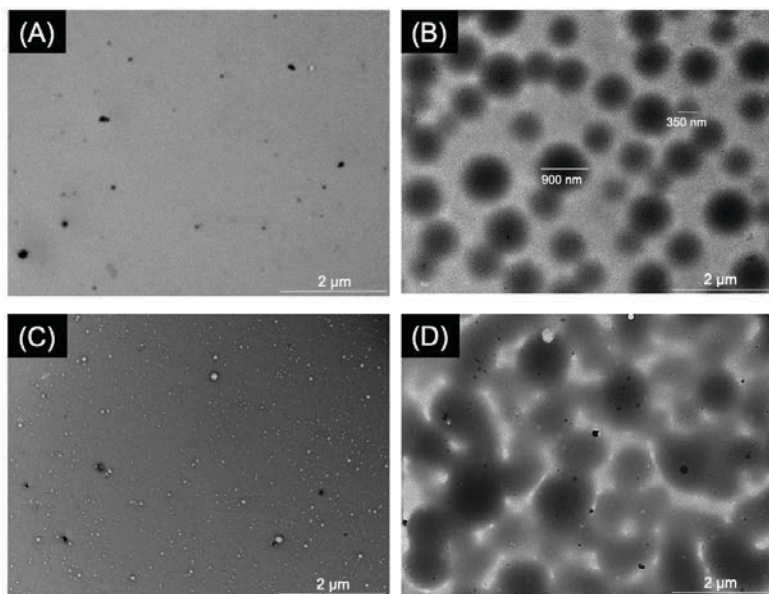

Figure S15. TEM images. MW-(ELP[V$_3$M$_1$-60])-(ELP[I$_1$-20])-C(*N*-EtSucc) solution in UP water at 0.1 % w/v, cooled **(A)** and heated **(B)**. PTMC$_{30}$-*b*-MW-(ELP[V$_3$M$_1$-60])-(ELP[I$_1$-20])-C(*N*-EtSucc) solution in UP water at 0.1% w/v, cooled **(C)** and heated **(D)**. Images size: 2 µm.

It is important to precise that TEM preparation procedures prevent an accurate control of the local concentration and temperature of the samples. Nevertheless, the pictures obtained for the diblock and triblock were consistent with their intrinsic characteristics: at low temperature, the MW-(ELP[V$_3$M$_1$-60])-(ELP[I$_1$-20])-C(*N*-EtSucc) diblock showed mostly nothing except some aggregates which is probably due to the uncontrolled TEM sample or some impurities. For sample prepared at high temperature, similarly to AFM images, a phase transition occurred leading to

microscale coacervation phenomenon due to the diblock change of solubility. For the triblock PTMC$_{30}$-*b*-MW-(ELP[V$_3$M$_1$-60])-(ELP[I$_1$-20])-C(*N*-EtSucc) image at low temperature (Figure S15C), small nanoparticles of approximately 30 nm were visible, characteristic of a self-assembly of the triblock and consistent with liquid AFM images. Those micelles turned to connected microscale spheres when heated above the Tt. Like the diblock, coacervates were formed when the temperature of the solution exceeded the BC blocks Tt. However, these coacervates were bridged by the hydrophobic ELP[I$_1$-20] segments, resulting in the interconnected network displayed in Figure S15D.
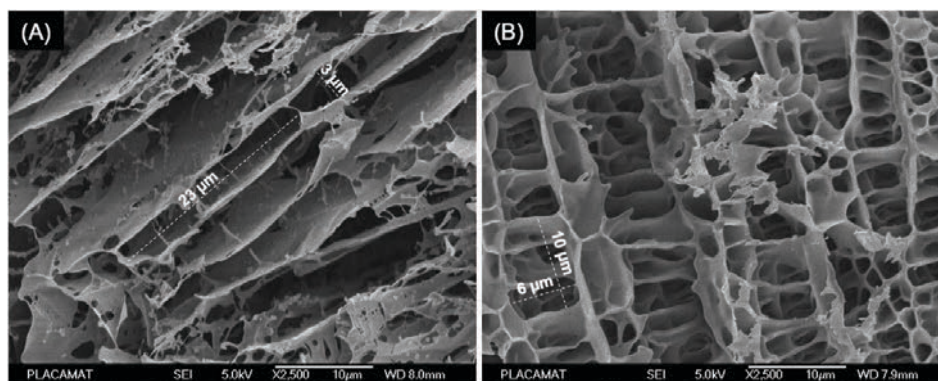

Figure S16. Cryo-SEM images of heated and sublimated PTMC$_{30}$-*b*-MW-(ELP[V$_3$M$_1$-60])-(ELP[I$_1$-20])-C(*N*-EtSucc) solution in UP water **(C)** at 4 % w/v. and **(D)** at 8 % w/v. Scale bar = 10 µm.

Video S1. Formation of coacervates from a diblock MW-(ELP[V$_3$M$_1$-60])-(ELP[I$_1$-20])-C(*N*-EtSucc) solution at 5 % w/v upon heating above its Tt (4 – 35 °C).

Video S2. Formation of coacervate structures from triblock PTMC$_{30}$-*b*-MW-(ELP[V$_3$M$_1$-60])-(ELP[I$_1$-20])-C(*N*-EtSucc) solution at 5 % w/v phase upon heating above its Tt (4 – 25 °C).